RESPONSE TO REFEREE#1 COMMENTS AND PEER-REVIEW REPORT

Manuscript Title: **"The Electrical Activity of Saharan Dust as perceived from Surface Electric Field Observations in Greece"**

Authors (as declared in the submitted manuscript with an addition of Ms. Ioanna Tsikoudi, justified contribution to the *declaration of author contributions*):

Vasiliki Daskalopoulou, Sotirios A. Mallios, Zbigniew Ulanowski, George Hloupis, Anna Gialitaki, Ioanna Tsikoudi, Konstantinos Tassis and Vassilis Amiridis

Dear respected Editor/Reviewers,

The authors highly appreciate the comprehensive feedback throughout the review process and kindly integrate the reviewer comments in the revised preprint manuscript, as follows:

REFEREE#1 COMMENTS:

"Major comments:
1.The title does not exactly reflect the contents of the manuscript. The manuscript, apart from the surface E-field observations mentioned in the title, also presents height profiles of dust AND e-field modelling. "The electrical activity of Saharan dust" suits better the contents to my taste."

Author's Response: We highly appreciate the insightful comment on the paper title, which indeed would describe the context in a broader manner, but in our effort to highlight the synergistic measurements of the ground E-field and particle optical properties, but also point out that the attempt for a distinction of electrically active dust is done only by surface E-field observations, the authors would like to keep the title as is. We have, however, excluded the geographical information which we find limiting of our methodology. Therefore:
Title from: **"The Electrical Activity of Saharan Dust as perceived from Surface Electric Field Observations in Greece"**
is changed to **"The Electrical Activity of Saharan Dust as perceived from Surface Electric Field Observations"**

2. The different Y-axes in Figs. 4-7 of the E-field, make it extremely difficult for (or even deter) the reader to compare the observations."

Author's Response: Figures 4 to 7 (revised as Fig. 6 to Fig. 9) have been adequately changed to the same Y-axis limits. Multi-panel Figure 14 (revised to Fig. 11) has been kept with the max E-field values for each dust event in order to: i. fully exploit the min/max range of the measured field for each event, ii. to highlight the comparison between the derived mean E-field (black line) with the reference field (red line), which is one of the key features of the study and lastly, iii. to enhance the visual comparison between the E-field diurnal variation and the dust layer bottom base throughout the day.

"Minor comments:
Lines 37-39: The statement that "The Global Electric Circuit (GEC) is an electrical circuit, and specifically a spherical capacitor that is formed between two conducting planes, with one being the Earth's surface, a good conductor of electricity, and the other the Ionosphere" is not correct. The GEC CAN BE THUS COCEPTUALISED but it IS NOT what it is stated. Please rephrase."
Author's Response: Thank you again for the comment, we have modified **Lines 38-42** as:

"The Global Electric Circuit (GEC) represents the electric current pathway in the Earth's atmosphere. The electric current that flows upwards from thunderstorms and electrified clouds into the Ionosphere, spreads out over the globe along magnetic field lines to the opposite hemisphere, and returns to the surface of the Earth as the fair weather air-Earth current (Bering et al, 1998). The GEC is established by the conducting atmosphere sandwiched between the conductive Earth and the conductive Mesosphere/Ionosphere (Williams, 2009)."

References (*not previously included in the manuscript*):

Bering III, E.A., Few, A.A., Benbrook, J.R., The global electric circuit, Phys. Today, 51, 24–30, 1998.

Williams, E.R., The global electric circuit: A review, Atmos. Res., 91, doi:10.1016/j.atmosres.2008.05.018, 2009.

Line 40: "GEC, greatly depend on ambient weather conditions and convective meteorological systems...", a passing reference here would also be Kourtidis et al., The influence of circulation weather types on the exposure of the biosphere to atmospheric electric fields, International Journal of Biometeorology DOI: 10.1007/s00484-020-01923-y

Line 40, modified to **Line 44:** added the respective reference as (Kourtidis et. al, 2020), thank you for the kind suggestion.

References (*not previously included in the manuscript*):

Kourtidis, K., Szabóné André, K., Karagioras, A., Nita, I. A., Sátori, G., Bór, J. and Kastelis, N.: The influence of circulation weather types on the exposure of the biosphere to atmospheric electric fields, Int. J. Biometeorol., doi:10.1007/s00484-020-01923-y, 2020.

Lines 85-86 "In this study, we focus on monitoring perturbations of the E-field near the ground caused by the transported dust layers, with special emphasis on slow E-field perturbations (with period larger than 6 hours), …": Period or duration?

Lines 90: we have changed the word "period" to "duration".

Lines 91-92: "by the ground-based electrometer " ! "by ground-based electrometers".

Lines 91-92 updated to **Lines 95-96:** added the word "same" as "by the same ground-based electrometer", as it was the same instrument that we re-located from Finokalia to Antikythera station.

Lines 106 "are prevalent during the intermediate season ": which season is that? Please clarify.

Line 106 updated to **Line 111:** added the phrase "of March till June" as in "are prevalent during the intermediate season of March till June"

Line 128-129 "VLDR is defined as the ratio of the cross–polarized to the parallel-polarized backscattered signal…and typical pure dust values are between 30% - 40% …": Please give some information also on VLDR values for mixed dust as well as VLDR values above 40%.

Author's Response: The authors have re-evaluated the Volume Linear Depolarization Ratio (VLDR) range of values, as the ones used in the pre-print version were characteristic of the Particle Linear Depolarization Ratio (PLDR) used in earlier stages of this research. Moreover, during the review process of the manuscript, the Polly^{XT} lidar underwent a refined polarization calibration process that altered the values used for the derivation of the PLDR and the data were, thereafter, processed uniformly with the Single Calculus Chain (SCC) algorithm (D'Amico et al., 2015) of EARLINET. Therefore, we have

incorporated the novel plots to the final version of the manuscript and in order to further strengthen dust layer characterization, we have calculated profiles of the particle backscatter coefficient (β) and the PLDR (referred to as δ_p in the revised manuscript), averaged for timeframe when dust episodes were fully developed. We, have therefore carefully inspected the manuscript and corrected the aerosol subtypes within the following ranges (Veselovskii, 2016, 2020).

- PLDR values for pure Saharan dust: 25 – 35% at 532nm
- VLDR values above 15% at 532nm, are indicative of dust presence (i.e. mixtures of dust with weakly depolarizing aerosols such as marine or smoke particles)

Renewed Plot example:

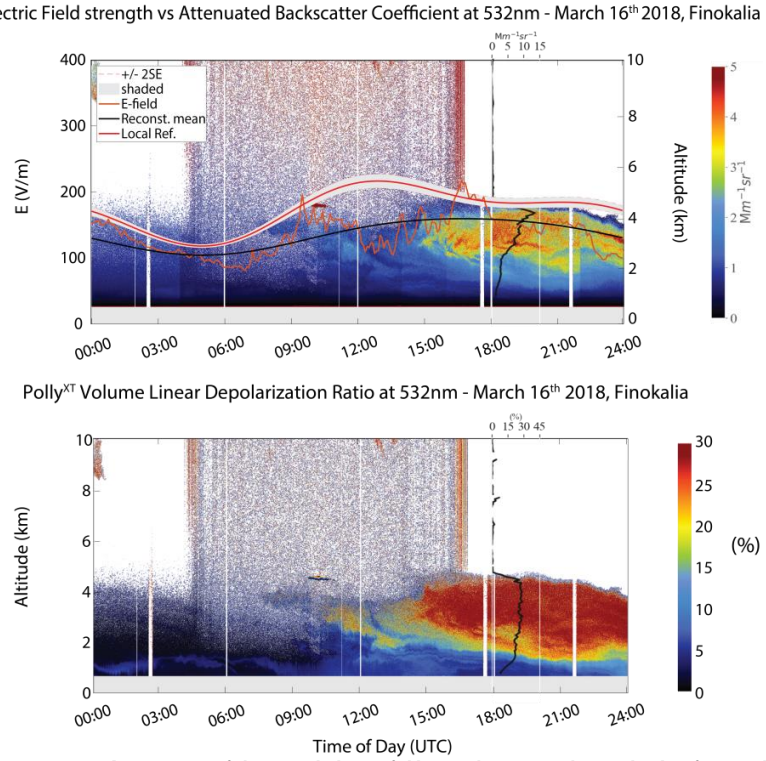

Fig. 8. Top panel: Timeseries of the vertical electric field strength (orange), the Localized Reference Electric Field (red) and the reconstructed mean electric field variation (black) plotted with the time-height evolution of the attenuated backscatter coefficient ($Mm^{-1}sr^{-1}$) and the particle backscatter coefficient (β) profile ($Mm^{-1}sr^{-1}$, black vertical line) averaged between 18:00 and 21:00 (UTC), for the 16/03/2018 dust layer in Finokalia station. Areas of increased particle concentration are denoted with red tones, while the β values reach up to 15 ($Mm^{-1}sr^{-1}$). The mean E-field remains positive but well below the reference field, exhibiting an increase as particle injection initiates at ~11:00 (UTC) and then a decrease along the plume's progression. **Bottom panel:** Volume Linear Depolarization Ratio (VLDR, %) for

the same dust layer as obtained from the Polly^{XT} lidar and the Particle Linear Depolarization Ratio (PLDR, %) profile (black vertical line). VLDR values close to 30% are indicative of high dust particle concentration and PLDR values persistently of 30% are characteristic of pure dust within the entirety of the layer (1-4 km).

All related paragraphs and figure captions within the text have been updated respectively. More specifically:

- **Lines 124-129:** modified to Paragraph from **Line 129** to **Line 142** as "The system employs two detectors, … of substantial particle concentrations (Haarig et al., 2017; Veselovskii et al., 2016, 2020)."
- **Lines 262-270:** modified to Paragraph from **Line 370** to **Line 388** as "The July 2017 and March 2018 dust events…, are also present within the MABL."
- **Fig. 4** (renewed Fig. 6) caption in **Lines 788-795**: "Top panel: Timeseries of the vertical electric field… δp values between 25% - 30% in the afternoon are characteristic of pure dust."
- **Fig. 5** (renewed Fig. 7) caption in **Lines 799-807**: "Top panel: Timeseries of the vertical electric field… δp values between 25% - 30% in the afternoon are characteristic of pure dust."
- **Fig. 6** (renewed Fig. 8) caption in **Lines 811-819**: "Top panel: Timeseries of the vertical electric field… PLDR values persistently of 30% are characteristic of pure dust within the entirety of the layer (1-4 km)."
- **Fig. 7** (renewed Fig. 9) caption in **Lines 823-831**: "Top panel: Timeseries of the vertical electric field… δp values between 25% - 30% in the afternoon are characteristic of pure dust."

Reference:

D'Amico, G., Amodeo, A., Baars, H., Binietoglou, I., Freudenthaler, V., Mattis, I., Wandinger, U., and Pappalardo, G.: EARLINET Single Calculus Chain – overview on methodology and strategy, Atmos. Meas. Tech., 8, 4891–4916, https://doi.org/10.5194/amt-8-4891-2015, 2015.

References (*not previously included in the manuscript*):

Veselovskii, I., Goloub, P., Podvin, T., Bovchaliuk, V., Derimian, Y., Augustin, P., Fourmentin, M., Tanre, D., Korenskiy, M., Whiteman, D. N., Diallo, A., Ndiaye, T., Kolgotin, A. and Dubovik, O.: Retrieval of optical and physical properties of African dust from multiwavelength Raman lidar measurements during the SHADOW campaign in Senegal, Atmos. Chem. Phys., 16(11), 7013–7028, doi:10.5194/acp-16-7013-2016, 2016.

Veselovskii, I., Hu, Q., Goloub, P., Podvin, T., Korenskiy, M., Derimian, Y., Legrand, M. and Castellanos, P.: Variability in lidar-derived particle properties over West Africa due to changes in absorption: Towards an understanding, Atmos. Chem. Phys., 20(11), 6563–6581, doi:10.5194/acp-20-6563-2020, 2020.

Line 155, for LREF: "The specific reference field represents the electric field behavior under local fair weather conditions, …", but at line 158 "the local fair weather days are classified as the less electrically disturbed days, …". So, does LREF represent fair weather days or not so unfair weather days? Also, it is not so clear to me what do the authors mean by fair weather. I am unclear about whether they mean days representative of GEC influence.

Authors' Response: The Carnegie Vessel cruises retrieved the first ship-borne measurements of the PG which were processed by the Carnegie Institute researchers back in the early 20th century. The lack of consistent meteorological parameters monitoring along the cruises could not enable the characterization of fair weather days as what was later established by UK Met Office as "fair weather conditions" (Harrison, 2013). Therefore, fair weather days were selected as the representative days of the least electrically disturbed conditions, which is what we adopt also in the present work as fair weather. The proposed Reference field, as it omits fast perturbations (either from transient convective systems or extreme meteorological conditions that are translated to extreme E-field variabilities), represents the fitting to the local GEC influence without incorporating meteorological parameters (Shatalina, 2019). The subsequent necessity that arises for further validation of LREF through the

comparison to the fair weather field constrained by distinct meteorological criteria, similar to what is discussed in the work of Harrison and Nicoll (2018), is part of ongoing work undertaken by the authors.
Hence, the term of local fair weather days would be more clearly communicated by the term electrically fair weather days. In order to communicate the distinction more clearly, the authors have revised the following paragraph as suggested:

Modified Paragraph in Lines 152-161: From "For the classification of the behaviour of the vertical electric field under dust influenced conditions, as that of an enhanced, reduced or reversed E-field, … are clearly dominated by local influences (Harrison & Nicoll, 2018)." to:

Lines 165-175: "The classification of the vertical electric field behavior under dust influenced conditions, as that of an enhanced, reduced or reversed E-field, necessitates comparison with the local long-term fair weather electric field. In order to represent solely the diurnal GEC influence at each observational site, away from electric generators perturbing the near ground E-field (e.g. Zhou and Tinsley, 2007), we construct a Localized Reference Electric Field (LREF) by exploiting only the timeseries inherent attributes and the measuring quantity itself, through the processing chain described below (Fig. 2). Various authors have presented different methodologies for determining fair weather conditions (e.g. Anisimov, 2014). For the specific study, the selected constraints of fair weather are based on the classification of fair weather days as the less electrically disturbed days, also assumed by the Carnegie Institute researchers (Harrison, 2013). Although, local effects on the E-field at each site can be of random nature (wind gusts, lightning strikes, radon emission and turbulent flows due to orography), the selection of fair weather data can be based on noise reduction by subtracting values which are clearly dominated by local influences and not directly addressing the meteorological criteria of fair weather (Harrison & Nicoll, 2018)."
References (*not previously included in the manuscript*):

Shatalina, M. V., Mareev, E. A., Klimenko, V. V., Kuterin, F. A. and Nicoll, K. A.: Experimental Study of Diurnal and Seasonal Variations in the Atmospheric Electric Field, Radiophys. Quantum Electron., 62(3), 183–191, doi:10.1007/s11141-019-09966-x, 2019.

Zhou, L. and Tinsley, B. A.: Production of space charge at the boundaries of layer clouds, J. Geophys. Res. Atmos., 112(11), 1–17, doi:10.1029/2006JD007998, 2007.

Line 168-169 "first five principal harmonics to the diurnal cycle of the electric field …": Please add something to help the reader understand why the diurnal cycle of the field should or could represented by 5 harmonics.

Author's Response: added the following sentences and restructured paragraph **Lines 162-170** "The FM data are…. in the following signal equation for S(t):" to:

Lines 179-189: "When representing the E-field diurnal variation by the Carnegie Curve, which is used consistently as a reference against locally measured atmospheric electricity parameters, the hourly variations of the field that shape the curve correspond to the 24, 12, 8, and 6-hour durations, as deduced from previous consistent observations of the Carnegie vessel (Harrison, 2013). The present study attempts to derive the local harmonic fit in the form of LREF, based on the form of the Carnegie curve, and assuming that this trend should be followed by the reference field as well. Consequently, the averaged 1s data to 1-minute data (datalogger configuration) are shifted to the frequency domain through a Fast Fourier Transform (FFT) representation so as to evaluate the relative contributions of the first five principal harmonics to the diurnal cycle of the electric field (hourly variations including daily mean), which are depicted in the following signal equation for S(t) (1). We note, that days with missing data are removed, because the uneven temporal distribution of the measurements modifies the time window for the FFT algorithm, and therefore, modifies the timeseries spectrum."

*Lines 174-175 "fi = i * (t/24) * 360 is the frequency of each harmonic ": is t the same as in eq. (1) above? If yes, then fi is a time-varying frequency? I believe t should be removed, else it results in terms of t^2 in (1). I believe the correct is fi = (i/24) * 360.*

Lines 174-175 updated to **Lines 189-191:** the presence of time t in Eq. (1) is a typographical error and therefore removed as follows:

$$S(t) = A_0 + A_1 cos(2\pi f_1 + \varphi_1) + A_2 cos(2\pi f_2 + \varphi_2) + A_3 cos(2\pi f_3 + \varphi_3) + A_4 cos(2\pi f_4 + \varphi_4)$$

where now the frequency f_i relates exactly to the given term as $f_i = i\frac{t}{24}360°, for\ i = 0, \dots 4$.

Line 171 updated to **Line 191:** changed sentence from "the electric field at time t in hrs" to "the electric field at time t in hrs (UTC)".

Line 204 "Under fair weather atmospheric conditions, complete lack of particles in the atmospheric circulation is expected ": Not by me. By whom is COMPLETE LACK of particles expected? I believe the sentence should be rephrased to a less emphatic form.

Authors' Response: We again thank the reviewer for the insightful comment, as we agree that under fair weather the electric field near the ground and in turn the air-Earth conduction current are strongly influenced by the variable concentration of aerosol particles (diurnal, annual and seasonal) (e.g. Siingh et al., 2009; Kastelis et al., 2016 and references therein), cloud droplets and water vapor, that in turn affect the ion attachment and recombination processes (e.g. Tinsley, 2006; Rycroft, 2008). Ideally, the complete lack of aerosols will lead to electrical properties (ion density, electric field) exactly the same as the unperturbed fair weather values. This means that the losses of the atmospheric ions are attributed only to the ion-ion recombination mechanism. As the concentration of the aerosols increases, perturbations from the fair weather values occur, since ion attachment to aerosols begins to become prominent. Nevertheless, as the reviewer states, there can be aerosol particles with concentrations that do not alter significantly the fair weather values.

Line 204: The sentence "Under fair weather atmospheric conditions, complete lack of particles in the atmospheric circulation is expected, except of ions." is replaced with updated:

Lines 222-227: "Ideally, under strict fair weather conditions, complete lack of aerosol particles in the atmospheric circulation is expected, since it guarantees that the only mechanism of atmospheric ions loss is the ion-ion recombination. As the concentration of aerosols increases, additional loss can be due to ions attaching to the particles, which leads to a perturbation of the ion density from fair weather values. In actual conditions, aerosols always exist, but under fair weather conditions their concentrations are small enough to not significantly affect the ionic content of the atmosphere. Therefore, for the modelling purposes of fair weather conditions, aerosol concentrations can be neglected."

References:

Siingh, D., Gopalakrishnan, V., Singh, R. P., Kamra, A. K., Singh, S., Pant, V., Singh, R. and Singh, A. K.: The atmospheric global electric circuit: An overview, Atmos. Res., 84(2), 91–110, doi:10.1016/j.atmosres.2006.05.005, 2007.

Kastelis, N. and Kourtidis, K.: Characteristics of the atmospheric electric field and correlation with CO 2 at a rural site in southern Balkans, Earth, Planets Sp., doi:10.1186/s40623-016-0379-3, 2016.

Line 209" near ground atmospheric conductivity and the atmospheric scale height...": So, you assume _ to be proportional to density, I guess. Perhaps you could add a line or two on the foundations of this assumption.

Author's Response: We thank the reviewer for this remark and have added the following sentence:

Modified **Line 209 to Lines 233-235**: "The given mathematical formalism of the atmospheric conductivity is adopted also by Ilin et al, 2020. The authors demonstrated that such a profile adequately describes the main aspects of the real conductivity distribution, and can be seen as a global mean conductivity profile."

Reference (*not previously included in the manuscript*):

Ilin N.V., Slyunyaev N.N., and Mareev E.A., Towards a realistic representation of global electric circuit generators in models of atmospheric dynamics, J. Geophys. Res. Atmospheres, 125, doi:10.1029/2019JD032130, 2020.

Line 246: A reference to Instructor's Solution Manual for Introduction to Electrodynamics, 4th Edition, 2013, is needed.

Line 246, updated to **Line 275:** corrected the reference from "Griffiths Instructor's Solutions Manual" to "Griffiths Instructor's Solution Manual for Introduction to Electrodynamics, 4th Edition, 2013".

Figure 1 could (and should, to my taste) be incorporated into Figs 4-7.

Author's Response: We think that Figures 4 to 7 (later revised to Fig. 6 to 8) are already clustered with information and potential incorporation of the HYSPLIT back trajectories will deter the reader from focusing on the E-field details and would rather highlight the dust layer origin and progression. Under the specific scope, the authors recommend that Figure 1 is kept as is.

Figs 4 and 5 captions "VLDR values between 25% and 30% indicate the presence of mostly mixed dust ", Figs 6 and 7 captions "VLDR values between 35% and 40% indicate a pure dust layer ": Values >30% but <35% indicating what?

Author's Response: Please refer to the **Line 128-129** previous comment response. We have corrected the VLDR values range for the different aerosol types on all figure captions and text highlights.

RESPONSE TO REFEREE#2 COMMENTS AND PEER-REVIEW REPORT

Manuscript Title: **"The Electrical Activity of Saharan Dust as perceived from Surface Electric Field Observations in Greece"**

revised per **reviewer#1** comments as:

"The Electrical Activity of Saharan Dust as perceived from Surface Electric Field Observations"

Authors (as declared in the submitted manuscript with an addition of Ms. Ioanna Tsikoudi, justified contribution to the declaration of author contributions):

Vasiliki Daskalopoulou, Sotirios A. Mallios, Zbigniew Ulanowski, George Hloupis, Anna Gialitaki, Ioanna Tsikoudi, Konstantinos Tassis and Vassilis Amiridis

Dear respected Editor/Reviewers,

The authors highly appreciate the comprehensive feedback throughout the review process and kindly integrate the reviewer comments in the revised preprint manuscript, as follows:

REFEREE#2 COMMENTS:

"The authors study four dust events in Greece, using a combination of ground-based electric field measurements and lidar.Â˘a The events involve dust that originated in the Sahara 48 to 72 hours previously.Â˘a Two of the events enhance the electric field relative to the reference fair weather field, and the other two events diminish the electric field.

This paper presents a simple model to describe these electrical effects.Â˘a There are two components of the model.Â˘a First, that the dust will reduce the conductivity in the region it occupies by scavenging ions; this effect occurs even with neutral dust particles. Â˘a Second, there could be regions of charged dust – this is modeled as cylinders of monopolar charge (there could be two cylinders, one of positive and one of negative charge). Some of the parameters for the model can be obtained from the lidar, while other parameters cannot be independently obtained.

Here is where I get lost.Â˘a I found the results section very hard to follow.Â˘a It appears to me the authors show experimental results for dust event (Figs 4-7), and then present results of the model under various parameters (Figs 8-13)."

Author's Response: The authors are grateful to the respected reviewer for the constructive comments, up to this point concerning the readability of the manuscript. We agree that the results section appeared perplexed to the first read, therefore we have strongly revised the structure of this section by keeping the synergistic observations between the E-field and the dust layer optical properties, which are the paper's highlighted significance to our perspective, and have given to the physical reasoning behind our findings, through the 1D model outputs, a separate section (section 3). We believe that according to the referee's guidelines this further fortifies the paper and clarifies the distinction the authors attempt to do for lofted electrified dust.

All the structural changes are listed under the respective comment sections in detail.

Line 258 updated to **Line 288:** Section 3 from "Results" becomes "Model outputs", where we keep only the model results for the different cylinder configurations.

Section 3 is now subdivided to the following paragraphs:

- **Lines 289 – 295:** introductory paragraph, "As a result of the mathematical formalism…distances."

- **Lines 323 – 333 & 346 – 352** become **Lines 296 – 311:** section **3.1 E-field below Fair weather field**, “In this section, we describe the possible cases under which lofted dust layers...lidar PLDR profiles (Table 1).”
- **Lines 353 – 390** modified to **Lines 312 – 346:** section **3.1.1 Balanced/Imbalanced dipole field below Fair weather**, “We consider the case of two oppositely charged cylinders …below the fair weather value”
- **Lines 391 – 393** become **Lines 347 – 349:** section **3.2 E-field above Fair weather field**, “We examine…the LREF.”
- **Lines 394 – 412** modified to **Lines 350 – 360: s**ection **3.2.1 Balanced/Imbalanced dipole field above Fair weather field**, “For the same…location (below point A).”

Section 4 named “Experimental Results” and is subdivided to:

- **Lines 259 – 261** modified to **Lines 343 – 366:** introductory paragraphs to the section, “The near ground electric… supported by the model configuration described in the previous sections.”
- **Lines 262 – 270** modified to **Lines 370 – 388:** section **4.1 Dust Layer characterization through lidar**, “The July 2017 and… very low concentrations of dust particles are also present within the MABL.”
- **Lines 271 – 279** modified to **Lines 389 - 399:** section **4.2 Local mean E-field behaviour**, “Considering the electrical properties… the expected fair weather value.”
- **Lines 283 – 295** become **Lines 400 – 414: s**ection **4.3 Observed E-field enhancement as compared to LREF**, “In Fig. 6 and Fig. 7… for even smaller charge separation distances.”
- **Lines 296 – 312** become **Lines 415 – 431:** section **4.4 Observed E-field reduction as compared to LREF**, “Several dust load cases…of the dust layer aloft.”
- **Lines 444 – 450** become **Lines 432 - 438:** section **4.5 Reversed E-field polarity**, “If a reversed polarity…to be electrified.”

Section 5 becomes the “Discussion” section and is subdivided to:

- **Lines 413 – 443** section 3.4.3 becomes **Lines 440 – 467** section **5.1 “E-field dependence on the bottom charged are height”**, kept as was in previous manuscript only section numbering changes.
- **Lines 452 – 463** become **Lines 471 – 482** section **5.2 Chauvenet criterion validity**, and is kept the same as in the previous manuscript, only section numbering changes.
- **Lines 464 – 477** become **Lines 483 – 496 s**ection **5.3 Generalization of the cylindrical model and the LREF methodology** and is kept the same as in the previous manuscript, only section numbering changes.

Lines 497 – 518: Section 6 as “Summary and Conclusions”, no changes only different numbering

“I do not think there is much interest in the results of the simple model under various parameters.Â˘a I think these figures and the associated text should be removed. Rather, I think they should focus (succinctly) on using the model to rationalize the experimental results.Â˘a This must be done much better in order for the paper to be publishable.”

Author’s Response: In this study, we also focus on the solution of the problem of charged cylindrical areas placed within a conducting medium, in order to simulate the charge structure within elevated dust layers and deduce the E-field behavior near the sensor. Since there is a lack of vertical mapping of these structures and only a recent study by Zhang and Zhou, 2020, attempted to construct a map of the electrical structure of dust storms through surface observations, we have selected this formalism to better represent our experimental findings and used it as a proof of concept for our conclusions. The model is indeed a simplistic approach to the structure of charged areas and is based on previously used geometries on cloud electrification, but never before on dust layers. Its purpose is to give physical insights regarding the parameters that influence the electrical properties of dust layers, rather than reproducing the measurements.

Therefore, we believe that it is imperative to maintain the model outputs that are used to rationalize the E-field behavior (previously Figures 9 to 12), but to comply with the referee’s kind comments and to diminish the size of relevant information within the main text, we have condensed the information of Fig. 9 – 10 to a single figure, now Fig. 4 (a & b) and that concerning the reduction of the E-field below the fair weather values contained in Fig. 11 – 12, to Fig. 5 (a & b) in section 3/Model outputs. Moreover, the authors consider the sensitivity study of the ground E-field to the basic parameters given in Eq. 11 (previously

section 3.3.1 Dust layer acting as a passive element, Fig. 8) to be redundant for the main text, but an important addition as to why the conductivity reduction factor plays a significant role in the E-field effects and the selection of n based on experimental data. As a result, the respective section is removed from the text and added to Appendix A.

More analytically the changes are:

Lines 319 – 322: "Following this formulation…separation distances" updated to **Lines 291 – 295**, section Model outputs.
Lines 355 – 345: added to **Appendix A** updated to **Lines 520 – 353**, as "Dust layer acting as a passive element"

Lines 280 – 282: "According to the effect…to the local field." updated to **Lines 364 – 3367** and added the phrase "Through these observations we attempt to provide evidence of electrically active dust only by ground-based methods."
updated Lines 426 – 430: added the following paragraph "Following the 1D model outputs for such a case (see Section 3.1.1), this observed reduction could be attributed to either electrically neutral dust aloft or to electrically active dust with the charged regions in relatively small separation distances within the layer. Under the electrically active dust case, a charge imbalance of less than 10%, can be adequate to interpret the observed reduction of the E-field below the LREF for even smaller separation distances. But the detection of such an E-field reduction below the LREF cannot conclusively characterize the electrical activity of the dust layer aloft."

updated Lines 458 – 459: added the phrase "As such, observations of enhanced E-field above the fair weather values, for dust driven days, can be reproduced only when an electrically active dust layer is transported above the fieldmill."

Reference:

Zhang, H. and Zhou, Y. H.: Reconstructing the electrical structure of dust storms from locally observed electric field data, Nat. Commun., 11(1), doi:10.1038/s41467-020-18759-0, 2020.

"Also, it is important to justify the assumptions in the model (this is much more important than the mathematical details, which they cover in great depth). – give physical reason why eqn 4 has this form – why do uncharged aerosol particles scavenge ions?Â˚a This is a key assumption for their model, as it leads to the reduction factor n, but its not clear to me that this is physically correct. The authors must provide strong evidence to support this."

Author's Response: Thank you again for the comments. We added the following sentences in **Line 209**, that explain the choice of conductivity distribution with form as in Eq. 4: "The given mathematical formalism of the atmospheric conductivity is adopted by Ilin et al, 2020. The authors demonstrated that such a profile adequately describes the main aspects of the real conductivity distribution, and can be seen as a global mean conductivity profile."

Reference (*not previously included in the manuscript*):

Ilin N.V., Slyunyaev N.N., and Mareev E.A., Towards a realistic representation of global electric circuit generators in models of atmospheric dynamics, J. Geophys. Res. Atmospheres, 125, doi:10.1029/2019JD032130, 2020.

Regarding Eq. 8., we rephrased **Lines 217 – 223** (updated to **Lines 243 – 251**) as follows:

"However, the presence of aerosols in the atmosphere and consequently dust particles, affects atmospheric conductivity (Siingh et al., 2007; Tinsley and Zhou, 2006; Zhou and Tinsley, 2007). Aerosols tend to scavenge atmospheric ions due to electrostatic interactions and ion thermal diffusion, leading to a reduction of the atmospheric ion density, and consequently of the atmospheric electrical conductivity. The process of ion attachment to aerosols has been exhaustively investigated in the past literature. A review paper by Long and Yao, 2010 contains a summary of all models and theories regarding the aerosol charging

by ions. The case of a steady state atmospheric desert dust layer that does not exhibit charge stratification is examined below. The layer acts as a passive electrical element (resistor), and reduces the fair weather atmospheric conductivity due to the ion attachment to dust particles, by a reduction varying factor *n*. Fig. 3b, represents the above layer configuration, where the new conductivity profile within the layer will be:"

Reference (*not previously included in the manuscript*):

Long Z, and Yao Q, Evaluation of various particle charging models for simulating particle dynamics in electrostatic precipitators, J. Aerosol Sci., 41, doi:10.1016/j.jaerosci.2010.04.005, 2010.

"And overall, I think the paper needs to be communicated much more clearly, and walk the reader through the results and the logic behind their ideas.Â˘a Figure captions should clarify what the data represents (cannot assume someone knows this).Â˘a As I said above, I got lost and couldn't understand things."

Author's Response: We would like to think that the present format of the paper is much more reader friendly and easy to follow from the wide scientific community of ACP.

Fig. 4 (previously Fig. 9 & 10) caption updated to: "Vertical electric field strength at ground level, $\boldsymbol{E_{z_0,dipole}}$, below the fair weather field, for a dipole of: (a) finite uniformly charged cylinders and (b) non uniformly charged cylinders exhibiting charge imbalance, within an elevated dust layer as a function of the cylinder radius $\boldsymbol{R}$. $\boldsymbol{E_{z_0,dipole}}$ is calculated for separation distances of 0 (electrically neutral dust), 100, 200, 400 and 800 m (balanced dipole case only) between the charged layers. As the separation distance increases, the E-field increases due to the stronger influence of the lower cylinder to the surface resistance as it moves towards the ground. In (b), the dipole exhibits charge imbalance as a relative charge density difference of 8%, with the upper negative cylinder having smaller charge density. As the charged layers move apart the E-field increases more rapidly than in (a) for the same separation distances, since the influence of the upper cylinder is dominant. The enhancement effect in both cases is not significant enough to overcome the fair weather values."

Fig. 5 (previously Fig. 11 & 12) caption updated to: "Vertical electric field strength at ground level, $\boldsymbol{E_{z_0,dipole}}$, for a dipole of: (a) finite uniformly charged cylinders and (b) non uniformly charged cylinders exhibiting charge imbalance, within an elevated dust layer as a function of the cylinder radius $\boldsymbol{R}$. $\boldsymbol{E_{z_0,dipole}}$ is calculated for separation distances over 1 km between the two charged layers. The influence of the lower cylinder to the ground E-field becomes more prominent as the separation distance increases. In (b), the dipole exhibits charge imbalance as a relative charge density difference of 8%, with the upper negative cylinder having smaller charge density. As the charged layers move apart the E-field increases more rapidly than in (a) for the same separation distances, since the influence of the upper cylinder is dominant. For these separation distances, the enhancement effect in both cases is significant enough to overcome the fair weather values."

Fig. 6 (previously Fig. 4) caption updated to: "Top panel: Timeseries of the vertical electric field strength (orange), the Localized Reference Electric Field (red) and the reconstructed mean electric field variation (black) plotted with the time-height evolution of the attenuated backscatter coefficient (1/Mm sr) and the Particle Backscatter coefficient (β) profile (1/Mm sr, black vertical line) averaged between 18:00 and 21:00 (UTC), for the 25/07/2017 dust layer in Finokalia station. Areas of increased particle concentration are denoted with reddish tones, while the β values are between 3 to 4 (1/Mm sr). The mean E-field appears enhanced and is above the reference field. Bottom panel: Volume Linear Depolarization Ratio (δ_v, %) for the same dust layer as obtained from the Polly^{XT} lidar and the Particle Linear Depolarization Ratio (δ_p, %) profile (black vertical line). High δ_v values (>17%) are indicative of dust particle presence and δ_p values between 25% - 30% in the afternoon are characteristic of pure dust."

Fig. 7 (previously Fig. 5) caption updated to: "Top panel: Timeseries of the vertical electric field strength (orange), the Localized Reference Electric Field (red) and the reconstructed mean electric field variation (black) plotted with the time-height plots of the attenuated backscatter coefficient (1/Mm sr) and the particle backscatter coefficient (β) profile (1/Mm sr, black

vertical line) averaged between 18:00 and 21:00 (UTC), for the 20/10/2018 dust layer in Antikythera station. Areas of increased particle concentration are denoted with red tones, while the beta values reach up to 5 1/Mm sr. The mean E-field appears enhanced and is consistently above the reference field showing an increase at ~21:00 (UTC), when dust deposition becomes prominent. Bottom panel: Volume Linear Depolarization Ratio (δ_v, %) for the same dust layer as obtained from the Polly^{XT} lidar and the Particle Linear Depolarization Ratio (δ_p, %) profile (black vertical line). High δ_v values (>20%) are indicative of dust particle presence and δ_p values between 25% - 30% in the afternoon are characteristic of pure dust."

Fig. 8 (previously Fig. 6) caption updated to: "Top panel: Timeseries of the vertical electric field strength (orange), the Localized Reference Electric Field (red) and the reconstructed mean electric field variation (black) plotted with the time-height evolution of the attenuated backscatter coefficient (1/Mm sr) and the particle backscatter coefficient (β) profile (1/Mm sr, black vertical line) averaged between 18:00 and 21:00 (UTC), for the 16/03/2018 dust layer in Finokalia station. Areas of increased particle concentration are denoted with red tones, while the β values reach up to 15 (1/Mm sr). The mean E-field remains positive but well below the reference field, exhibiting an increase as particle injection initiates at ~11:00 (UTC) and then a decrease along the plume's progression. Bottom panel: Volume Linear Depolarization Ratio (VLDR, %) for the same dust layer as obtained from the Polly^{XT} lidar and the Particle Linear Depolarization Ratio (PLDR, %) profile (black vertical line). VLDR values close to 30% are indicative of high dust particle concentration and PLDR values persistently of 30% are characteristic of pure dust within the entirety of the layer (1-4 km)."

Fig. 9 (previously Fig. 7) caption updated to: "Top panel: Timeseries of the vertical electric field strength (orange), the Localized Reference Electric Field (red) and the reconstructed mean electric field variation (black) plotted with the time-height evolution of the attenuated backscatter coefficient (1/Mm sr) and the particle backscatter coefficient (β) profile (1/Mm sr, black vertical line) averaged between 18:00 and 21:00 (UTC), for the 23/06/2019 dust layer in Antikythera station. Areas of increased particle concentration are denoted with yellow to reddish tones, while the β values are between 3 to 4 (1/Mm sr). The mean E-field is positive and consistently below the reference field, exhibiting an increase when particle injection begins towards noon and further drops as the layer progresses to lower altitudes. Bottom panel: Volume Linear Depolarization Ratio (δ_v, %) for the same dust layer as obtained from the Polly^{XT} lidar and the Particle Linear Depolarization Ratio (δ_p, %) profile (black vertical line). High δ_v values (>15%) are indicative of dust particle presence and δ_p values between 25% - 30% in the afternoon are characteristic of pure dust."

Fig. 10: added $E_{z_0,dipole}$ to the caption.

Fig. A1 (previously Fig. 8)**:** "…(d) the separation distance." to "…(d) the dust layer depth."

The Electrical Activity of Saharan Dust as perceived from Surface Electric Field Observations ~~in Greece~~

Vasiliki Daskalopoulou[1,2], Sotirios A. Mallios[2], Zbigniew Ulanowski[3,4], George Hloupis[5], Anna Gialitaki[2,6], Ioanna Tsikoudi[2,7], Konstantinos Tassis[~~7,~~8,9] and Vassilis Amiridis[2]

[1]Department of Physics, Faculty of Astrophysics and Space Physics, University of Crete, Heraklion GR-70013, Greece
[2]Institute for Astronomy, Astrophysics, Space Applications and Remote Sensing, National Observatory of Athens, Athens GR-15236, Greece
[3]Department of Earth and Environmental Sciences, University of Manchester, Manchester M13 9PL, UK
[4]British Antarctic Survey, NERC, Cambridge CB3 0ET, UK
[5]Department of Surveying and GeoInformatics Engineering, University of West Attica, Aegaleo Campus GR-12244, Greece
[6]Laboratory of Atmospheric Physics, Department of Physics, Aristotle University of Thessaloniki, Thessaloniki GR-54124, Greece
[7]Department of Environmental Physics and Meteorology, National and Kapodistrian University of Athens, Athens, Greece
[~~8~~]Department of Physics, and Institute for Theoretical and Computational Physics, University of Crete, Heraklion GR-70013, Greece
[8]Institute of Astrophysics, Foundation for Research and Technology-Hellas, Heraklion GR-71110, Greece

Correspondence to: Vassilis Amiridis (vamoir@noa.gr)

Abstract. We report on the electric field variations during Saharan dust advection over two atmospheric remote stations in Greece, using synergistic observations of the vertical atmospheric electric field strength (E_z) at ground level and the lidar-derived particle backscatter coefficient profiles. Both parameters were monitored for the first time with the simultaneous deployment of a ground-based field mill electrometer and a multi-wavelength polarization lidar~~a multiwavelength lidar system~~. The field mill timeseries are processed to extract the diurnal variations of the Global Electric Circuit and remove fast field perturbations due to peak lightning activity. In order to identify the influence of the elevated dust layers on the ground E_z, we extract a Localized Reference Electric Field from the timeseries that reflects the local fair weather activity. Then, we compare it with the reconstructed daily average behaviour of the electric field and the Saharan dust layers' evolution, as depicted by the lidar ~~system~~. The observed enhancement of the ~~Reported cases of enhanced~~ vertical electric field (up to ~ 100 V/m), for detached pure dust layers, suggests the presence of in-layer electric charges. Although higher dust loads are expected to result in such an electric field enhancement, episodic cases that reduce the electric field are also observed (up to ~ 60 V/m). To quantitatively approach our results, we examine the dependency of E_z against theoretical assumptions for the distribution of separated charges within the electrified dust layer. Electrically neutral dust is approximated by atmospheric conductivity reduction, while charge separation areas within electrically active dust layers are approximated as finite extent cylinders. This physical approximation constitutes a more realistic description of the distribution of charges, as opposed to infinite extent geometries, and allows for analytical solutions of the electric field strength, so that observed ~~electric field~~ variations during the monitored dust outbreaks can be explained.

Keywords: Dust Electrification; Atmospheric Electric Field Measurements; Reference Electric Field; Charge Separation;

1 ~~1~~ Introduction

The Global Electric Circuit (GEC) represents the electric current pathway in the Earth's atmosphere. The electric current that flows upwards from thunderstorms and electrified clouds into the Ionosphere, spreads out over the globe along magnetic field lines to the opposite hemisphere, and returns to the surface of the Earth as the fair weather air-to-Earth current (Bering et al., 1998). The GEC is established by the conducting atmosphere sandwiched between the conductive Earth and the conductive Mesosphere/Ionosphere (Williams, 2009). ~~The Global Electric Circuit (GEC) is an electrical circuit, and specifically a spherical capacitor that is formed between two conducting planes, with one being the Earth's surface, a good conductor of electricity, and the other the Ionosphere, a weakly-ionized plasma at ~80 km altitude (e.g., Rycroft et al., 2008).~~ Atmospheric electric parameters, such as the vertical Electric Field (E_z) and induced ~~air~~ air-~~to~~ to-Earth current (I_c) through the GEC, greatly depend on ambient weather conditions and convective meteorological systems (Kourtidis et al., 2020) due to the re-distribution of charged or uncharged aerosols and terrestrial radioactive particles in the Earth's atmosphere (Harrison and Ingram, 2005; Wright, 1933)~~(e.g. Harrison & Ingram, 2005; Scrase, 1935; Wright, 1933)~~. Under fair weather conditions, which are defined according to international standards as those with cloudiness less than 0.2, wind speed less than 5 m/s and the absence of fog or precipitation (Chalmers, 1967; Harrison and Nicoll, 2018), the atmospheric electrical circulation is dominated by the potential difference between the global capacitor planes (about 250 kV, e.g., Rycroft et al., 2008), which in turn generates the fair weather electric field, and consequently the fair weather electric current in the presence of the conducting atmosphere. An average current density of 2 pA/m^2 and a downward looking (by convention positive, e.g., Rakov ~~&~~ and Uman, 2003, pp.8) electric field equal to a typical value of about 130 V/m are expected, respectively (Rycroft et al., 2008). The daily variation of the global thunderstorm activity modulates the electric field strength and the resulting diurnal variation is represented by the Carnegie curve (Harrison, 2013).

Amongst the aerosols affecting the atmospheric electrical content (Whitby ~~&~~ and Liu, 1966), mineral dust represents one of the most significant contributors, along with volcanic ash (Harrison et al., 2010), due to its mineralogical composition that results in different electrical properties of the dust particles (Kamra, 1972) and its abundance in terms of dry mass (Tegen et al., 1997). During dust storms, dust devils and subsequent advection of elevated dust layers the electrical parameters can vary greatly from the values under fair weather conditions (Harrison et al., 2016; Renno and Kok, 2008; Zheng, 2013). It is well documented that over deserts the emission process of dust particles can generate large atmospheric electric fields (Esposito et al., 2016; Renno and Kok, 2008; Zheng, 2013) that affect their flow dynamics (Kok and Renno, 2006). Charged dust occurrences are recorded via ground-based methods also in destinations further away from the source (Harrison et al., 2018; Katz et al., 2018; Silva et al., 2016; Yair et al., 2016; Yaniv et al., 2017), while balloon-borne observations (Kamra, 1972; Nicoll et al., 2011) indicate that space charge is indeed persistent within lofted dust layers during their transport to long distances. The exact mechanisms that would explain and sufficiently describe the long-range electrification of dust are not clear yet, and remain under investigation. Major processes that are considered responsible for the electrification of dust

Formatted: Indent: Left: 0", Hanging: 0.13", Outline numbered + Level: 1 + Numbering Style: 1, 2, 3, … + Start at: 1 + Alignment: Left + Aligned at: 0.25" + Indent at: 0.5"

Field Code Changed

particles include ion attachment (Tinsley and Zhou, 2006) and particle-to-surface or particle-to-particle collisions, i.e. triboelectrification (Kamra, 1972; Lacks and Shinbrot, 2019; Waitukaitis et al., 2014). Such processes are claimed to have large impact on desert dust transport and its influence in climate and ecosystems through ~~lifecycle and its influence,~~ the retention of larger dust particles in the atmosphere (van der Does et al., 2018) ~~;~~, as well as to ~~such as the observed~~ particle vertical orientation with impact on radiative transfer (Bailey et al., 2008; Mallios et al., 2021; Ulanowski et al., 2007). ~~and the retention of larger dust particles in the atmosphere (van der Does et al., 2018; Ryder et al., 2018).~~

Ground-based electric field measurements can be indicative of the electrical behaviour of elevated dust layers. These measurements can provide useful information if they are combined with other retrievals on aerosol profiling (e.g. lidar, ceilometer) (Nicoll et al., 2020). However, features of E-field timeseries, such as the enhancement of the near-ground electric field during dust outbreaks, are still unexplained in broad literature (Yaniv et al., 2016, 2017). Observations of enhanced or even reversed E-field at the height of the ground-based sensor, e.g. an electrostatic fieldmeter, are attributed by Ette (1971) and Freier (1960) to charge separation within electrically active dust. According to several laboratory studies (Duff and Lacks, 2008; Forward et al., 2009; Inculet et al., 2006; Waitukaitis et al., 2014), charge transfer processes lead to smaller particles being negatively charged while larger particles tend to be positively charged, therefore charge separation within lofted dust layers is also possible due to the expected size selective gravitational settling that could stratify the fine and coarse mode particles (Ulanowski et al., 2007). An observed reduction of the E-field in a mountainous area is attributed to the superposition of two dust layers in different heights with respect to the ground-based sensor (Katz et al., 2018). Moreover, layers that exhibit large particle densities lead to more particles competing for the same amount of ions (ion-particle competition, e.g., Gunn, 1954; Reiter, 1992), hence they act as a passive element within the atmospheric circulation and can reduce the near-ground electric field. A similar reduction of the electric field can be expected whenever, for any reason, the charge separation does not occur. As an example, one can think meteorological conditions that force the particles to move randomly, cancelling their vertical movement and, therefore, the charge separation. ~~A similar reduction of the electric field is also expected when meteorological conditions create random particle movement that cancels out the vertical propagation and, subsequently, the stratification of charges.~~ Nonetheless, systematic profiling measurements are needed so as to fully characterize the electrical properties of the dust particles aloft, with respect to the locally occurring meteorological conditions.

In this study, we focus on monitoring perturbations of the E-field near the ground caused by the transported dust layers, with special emphasis on slow E-field perturbations (with duration larger than 6 hours to exclude phenomena with small timescales or local effects of random origin ~~period larger than 6 hours~~), and we attempt to classify and comment on the electrical activity of the dust layers. As electrically active we define the layers that exhibit charge separation and behave as electrostatic generators in the GEC, similarly to electrified shower clouds and thunderstorms (e.g., Mallios and Pasko, 2012). Conversely, electrically neutral are assumed to be the layers with no charge separation which, therefore, act as passive elements in the GEC, similarly to the non-electrified shower clouds (e.g., Baumgaertner et al., 2014). Four selected cases of Saharan dust plumes are examined, as captured over Finokalia and Antikythera atmospheric observatories by the same ground-based

electrometer, as well as by the sophisticated Polly^{XT} lidar system. In ~~section~~ Section 2~~2~~, we provide an overview of the instrumentation and measurement techniques, and specify the methods used to parameterize the electrical behaviour of the dust layers. In ~~section~~ Section 0~~3~~, we present the modelled E-field behaviour which is used as a proof of concept for the explanation of the E-field diurnal variation (relative to the local reference field), presented in the results section ~~is presented~~ along with the dynamic evolution of the dust episodes as revealed by the profiling information from the lidar. We further discuss whether the configuration of finite cylindrical charge accumulation regions, previously suggested for the representation of charge distributions within thunderclouds (Krehbiel et al., 2008; Riousset et al., 2007), is capable of reproducing our experimental results. Finally, we present our conclusions in ~~section~~ Section ~~5~~6.

2 Data and methodology

We analyse four Saharan dust outbreaks recorded over two observational sites in Greece. The first atmospheric monitoring station is situated in the remote location of Finokalia (35.338° N, 25.670° E) on the north eastern coast of Crete, with the nearest large urban center being the city of Heraklion located 70 km to the west. The station is located at the top of a hill (252 m asl) facing the sea within a sector of 270° to 90° and the climatic characteristics are typical of the eastern Mediterranean basin exhibiting two distinctive seasons, the dry season (April to September) characterized by increased levels of pollution and biomass burning and the wet season (October to April). Significant Saharan dust transport occurs when S/SW winds are prevalent during the intermediate season of March till June and may lead to ground concentrations exceeding 1 mg/m^3 (Solomos et al., 2018). Since there is no significant human activity occurring at a distance shorter than 15 km within the above sector, it makes it an appropriate location for monitoring dust layers advected directly from the Sahara. The second site is the PANhellenic GEophysical observatory (PANGEA) in the remote island of Antikythera (35.861° N, 23.310° E, 193 m asl). The island covers an area of just 20.43 km^2, 38 km south-east of the larger island of Kythera and is devoid of human activity as its inhabitants are at most twenty people during early fall to mid-summer. The station location is ideal as the island is placed at a crossroad of air masses (Lelieveld et al., 2002), with NNE winds being prominent between August and February, while in spring and early summer western airflows that favor dust transport are observed. Moreover, the prevailing meteorological conditions on the island are again representative of the eastern Mediterranean with warm and dry days in summer in contrast to winter, when the days are colder and wetter days are typical. The dust outbreaks recorded were on the 25th of July 2017 and March 16th 2018 on Finokalia, October 20th 2018 and June 23rd 2019 on Antikythera, selected due to the presence of elevated dust layers in the lidar profiles.

2.1 Aerosol monitoring and characterization

2.1.1 Lidar measurements

For the comprehensive characterization of dust particle optical properties, we exploit the ~~vertical~~ profiling capabilities of the Polly^{XT} Raman ~~scattering~~ polarization lidar (Engelmann et al., 2016) of the National Observatory of Athens (NOA), as part of

Formatted: Indent: Left: 0", Hanging: 0.13", Outline numbered + Level: 1 + Numbering Style: 1, 2, 3, … + Start at: 1 + Alignment: Left + Aligned at: 0.25" + Indent at: 0.5"

Formatted: Indent: Left: 0", Outline numbered + Level: 2 + Numbering Style: 1, 2, 3, … + Start at: 1 + Alignment: Left + Aligned at: 0.25" + Indent at: 0.5"

Formatted: No underline

Formatted: Heading 3, Indent: Left: 0", Hanging: 0.31", Outline numbered + Level: 3 + Numbering Style: 1, 2, 3, … + Start at: 1 + Alignment: Left + Aligned at: 0.25" + Indent at: 0.75"

the European Aerosol Research Lidar Network (EARLINET). This multi-wavelength system is equipped with three elastic channels at 355, 532 and 1064 nm, two ~~rotational~~/vibrational Raman channels at 387 and 607 nm, two channels for the detection of the cross-polarized backscattered signal at ~~two linear depolarization channels at~~ 355 and 532 nm, and one water vapour channel at 407 nm. The system employs two detectors.~~Combined use of its~~ a near-field and a far-field telescope~~s~~ provide~~s~~ reliable aerosol optical property profiles from close to the ground to the upper troposphere.~~vertical profiles from 0.25 km to 10 km in height.~~ The basic lidar quantities used for the monitoring and characterization of dust loads in our study, are the total attenuated backscatter coefficient ($Mm^{-1}sr^{-1}$) at 532 nm (calibrated range-corrected signal) to account for particle concentrations and the Volume Linear Depolarization Ratio (VLDR, δ_v) at 532 nm.~~of dust loads and as much as possible pure ones, are the Total Attenuated Backscatter coefficient (1/msr) at 1064 nm (calibrated and range corrected signal) for lofted particle concentrations and the calibrated Volume Linear Depolarization Ratio (VLDR) at 532 nm for the characterization of aerosol types.~~ VLDR (%) is ~~defined as~~ the ratio of the cross–polarized to the ~~parallel~~co-polarized backscattered signal (Freudenthaler et al., 2009), where cross- and co- are defined with respect to the plane of polarization of the emitted laser pulses. It encloses the influence of both atmospheric particles and molecules, with high δ_v values being indicative of irregular particles (i.e. atmospheric dust). However, for a comprehensive aerosol characterization, the particle backscatter coefficient (β) and Particle Linear Depolarization Ratio (PLDR, δ_p) are needed. PLDR (%) is derived from VLDR by correcting for molecular depolarization with atmospheric parameters extracted from radiosonde measurements (i.e. atmospheric pressure and temperature). In the selected case studies, we also present the δ_p and β profiles, as derived in the timeframe when each dust episode was fully developed (averaged between 18:00 and 21:00 (UTC) for all dust cases). Typical δ_p values for Saharan dust are in the range of 25% to 35% at 532 nm, while large β values are representative of substantial particle concentrations ~~and typical pure dust values are between 30% - 40%~~ (Haarig et al., 2017; Veselovskii et al., 2016, 2020).

2.1.2 Ancillary aerosol and trajectory information

The Aerosol Optical Depth (AOD) was monitored by a CIMEL sunphotometer, part of the Aerosol Robotic Network (AERONET - https://aeronet.gsfc.nasa.gov/), which was co-located with the lidar on both stations. For the cases examined here, the AOD varied from 0.221 to 0.366 at 500 nm. To characterize the air masses in regard to their origin we use the NOAA HYSPLIT back trajectory model, driven by GDAS meteorological data (https://www.ready.noaa.gov/HYSPLIT.php). The arrival heights for dust over the observational sites were selected in HYSPLIT according to the prevailing layering depicted by our lidar measurements (Fig. 1).

2.2 Electric Field measurements and data processing

2.2.1 Ground-based E-Field measurements

The JCI 131 Field mill (FM) electrometer (Chubb, 2014; Chubb, 2015) was installed in Finokalia from April 2017 until May 2018 (382 days) and then re-located to Antikythera, where the examined timeseries span from June 2018 to June 2019 (243 days) for continuous monitoring of the near-ground (on instrument mast height) vertical electric field. Field mills are robust

Formatted: Font: Bold, No underline

Formatted: Heading 3, Indent: Left: 0", Hanging: 0.31", Outline numbered + Level: 3 + Numbering Style: 1, 2, 3, … + Start at: 1 + Alignment: Left + Aligned at: 0.25" + Indent at: 0.75"

Formatted: No underline

Formatted: Indent: Left: 0", Outline numbered + Level: 2 + Numbering Style: 1, 2, 3, … + Start at: 1 + Alignment: Left + Aligned at: 0.25" + Indent at: 0.5"

Formatted: No underline

Formatted: Heading 3, Indent: Left: 0", Hanging: 0.31", Outline numbered + Level: 3 + Numbering Style: 1, 2, 3, … + Start at: 1 + Alignment: Left + Aligned at: 0.25" + Indent at: 0.75"

instruments, mostly used for lightning warning applications providing, though, sufficient sensitivity for the detection of weaker electric fields. The instrument was mounted on a 3 m pole, and as far as possible from physical obstacles, buildings and any metallic objects that could create distortions to the electric field. However, on Finokalia the FM was on the edge of a hilly elevation which added a topography factor, not quantified in the specific research due to the lack of typical flat ground measurements in the area. On Antikythera, the mill installation location could be more carefully selected to avoid orography, obstacles and power grid lines. Instrument output range was set to the most sensitive scale (2.0 kV full scale) with a sensitivity of the order of 1 V/m for 1 Hz measurement frequency and the data were acquired from a 24-bit local data-logger. In order to interpret the field mill measurements, it is essential to compare the data with a reference field representative of local fair weather conditions. The methodology followed for this process is described in the paragraph below.

2.2.2 Derivation of the Localized Reference Electric Field

Formatted: Font: Bold, No underline

Formatted: Heading 3, Indent: Left: 0", Hanging: 0.31", Outline numbered + Level: 3 + Numbering Style: 1, 2, 3, … + Start at: 1 + Alignment: Left + Aligned at: 0.25" + Indent at: 0.75"

For tThe classification of the behaviour of the vertical electric field behaviour under dust influenced conditions, as that of an enhanced, reduced or reversed E-field, necessitates comparison with the local long-term fair weather electric field is required. In order to represent solely the diurnal GEC influence at each observational site, away from electric generators perturbing the near ground E-field (e.g., Zhou and Tinsley, 2007).For this purpose, we construct a Localized Reference Electric Field (LREF) by exploiting only the timeseries inherent attributes and the measuring quantity itself,is constructed from the determination of local fair weather conditions, prevalent for each station, through the following processing chain described below (Fig. 2). Various authors have presented different methodologies for determining fair weather conditions (e.g., Anisimov et al., 2014). For the specific study, the selected constraints of fair weather are based on the classification of fair weather days as the less electrically disturbed days, also assumed by the Carnegie Institute researchers (Harrison, 2013b).

Instead of eliminating meteorological disturbances (except for lightning activity) for the retrieval of global information of the fair weather E-field (Harrison & Nicoll, 2018), the local fair weather days are classified as the less electrically disturbed days, based on the measured quantity itself through the construction of the reference field. Although, the local effects on the E-fieldE_z at each site can be of random nature (wind gusts, lightning strikes, radon emission and turbulent flows due to orography), the selection of fair weather data can be based on the noise reduction by subtracting valuesof random local noise by first removing values which are clearly dominated by local influences and not directly addressing the meteorological criteria of fair weather (Harrison and Nicoll, 2018).

As such, Tthe FM data are pre-processed by applying the appropriate scaling factor for the 3 m mounting mast of the electrometer (Chubb, 2015) and then days with no missing values due to either instrument malfunction, power outages or pc communication failures, are selected (Filter no. 1). Under local fair weather conditions, the E-field, as measured here, is positive therefore imposing the second filtering step with a non-negativity constraint (Filter no. 2). When representing the E-field diurnal variation by the Carnegie Curve, which is used consistently as a reference against locally measured atmospheric electricity parameters, the hourly variations of the field that shape the curve correspond to the 24, 12, 8, and 6-hour durations, as deduced from previous consistent observations of the Carnegie vessel (Harrison, 2013b). The present study attempts to

derive the local harmonic fit in the form of the LREF, based on the Carnegie curve morphology, and assuming that this trend should be followed by the reference field as well. Consequently, the averaged 1s data to 1-minute data (datalogger configuration) are shifted to the frequency domain through a Fast Fourier Transform (FFT) representation so as to evaluate the relative contributions of the first five principal harmonics to the diurnal cycle of the electric field (hourly variations including daily mean), which are depicted in the following signal equation for $S(t)$ (1). ~~(Harrison, 2013).~~ We note, that days with missing data are removed, because the uneven temporal distribution of the measurements modifies the time window for the FFT algorithm, and therefore, modifies the timeseries spectrum. ~~These are depicted in the following signal equation for $S(t)$:~~

$$S(t) = A_0 + A_1\cos(2\pi f_1 t + \varphi_1) + A_2\cos(2\pi f_2 t + \varphi_2) + A_3\cos(2\pi f_3 t + \varphi_3) + A_4\cos(2\pi f_4 t + \varphi_4) \quad (1)$$

where S is the electric field at time t in hrs (UTC), A_i for $i = 0,..4$ ~~where~~ with A_0 ~~represents~~ representing the mean value (constant, zeroth harmonic) and A_1 to A_4 (first to fourth harmonic) represent the amplitudes of the 24, 12, 8, and 6-hour variations, $f_i = i\frac{t}{24}360^\circ$ is the frequency of each harmonic, where $f_0 = 0$ and φ_i are the respective phases in degrees, with $\varphi_0 = 0$ (Harrison, 2013). Based on the form of the Carnegie curve, and assuming that this trend should be followed by ~~the reference field as well~~LREF, we find empirically that the ratio between the zeroth harmonic and the first harmonic is around ~~2~~two. Therefore, the E_z values for which the amplitude A_0 is larger than two times the amplitude A_1 are kept (Filter no. 3). The same filter is applied to the other harmonics as well (A_0 is larger than two times the A_i), making sure that no~~t~~ ~~fast~~ fast-transient contribution is kept.

Lastly, since the amplitude of each harmonic is expected to be constant for all days (as the amplitudes in the Carnegie curve do), we impose the Chauvenet criterion on each of the filtered five harmonics amplitude, so as to detect outliers. The criterion is imposed once with the use of the relation below:

$$N\,erfc\left(\frac{d^j}{\sqrt{2}s}\right) < \frac{1}{2} \quad (2)$$

~~for a deviation of:~~where

$d^j = \left|{A_i}^j - \bar{A}_i\right|$, is the deviation for $i = 0,..4$ referring to the i[th] harmonic, $j = 0,..N$ the day number and N the total number of days, for:

~~where $i = 0,..4$ refers to the i[th] harmonic, $j = 0,..N$ day number and N the total number of days, for~~

$\bar{A}_i = \frac{1}{N}\sum_{j=1}^{N} {A_i}^j$, where A_{ij} is the i[th] harmonic amplitude per day and summated over j gives $\bar{A}_i$ as the mean amplitude of each harmonic.

~~where A_{ij} is the i[th] harmonic amplitude per day and summated over j gives $\bar{A}_i$ as the mean amplitude of each harmonic.~~ Lastly, s is the unbiased sample variance and is defined as:

$$s^2 = \frac{\sum_{j=1}^{N}\left({A_i}^j - \bar{A}_i\right)^2}{N-1}$$

within erfc(x) ~~is~~ which is the complementary error function, defined as:

Field Code Changed

Formatted: Indent: Left: 0.36", Right: -0.38"

Formatted: Indent: Left: 0.36"

Formatted: Indent: Left: 0", First line: 0.38"

Formatted: Indent: First line: 0.38"

Formatted: Indent: Left: 0", First line: 0.38"

$$erfc(x) = 1 - erf(x) = 1 - \frac{2}{\sqrt{\pi}} \int_0^x e^{-t^2} dt$$

~~Also *s* is the unbiased sample variance and is defined as:~~

$$s^2 = \frac{\sum_{j=1}^{N} \left(A_i{}^j - \bar{A}_i\right)^2}{N-1}$$

After the Chauvenet criterion is met, 152 total undisturbed weather days are detected for Finokalia and 109 days for Antikythera. From this reduced dataset, we reconstruct the LREF by keeping the mean values of the first three harmonics and calculate the respective standard errors as ±2SE from the reconstructed signal.

2.2.3 E-field measurement comparison

In order to compare LREF with the daily variation of the electric field during the dust events, these field mill measurements are also shifted to the frequency domain through an FFT. Again, the first five harmonics are retained and from the specific dataset, a smoothed slow varying field is reconstructed (otherwise referred to as reconstructed mean for the remainder of this paper) from the set of mean amplitudes and phases of the first three harmonics. This filtered field retains the main characteristics of the local reference field~~.~~, since fast transient events which are less than 6 hrs in duration are removed. Therefore, the LREF and reconstructed mean field signals that are compared have the same spectral information. ~~In order to~~Moreover, to compare ~~plot~~ the E-field timeseries with the ~~total attenuated backscatter coefficient~~lidar retrievals, all the field mill data are further averaged to 5 mins.

2.3 Mathematical formalism for the modelling of the ground E-field

Ideally, under strict fair weather conditions, complete lack of aerosol particles in the atmospheric circulation is expected, since it guarantees that the only mechanism of atmospheric ions loss is the ion-ion recombination. As the concentration of aerosols increases, additional loss can be due to ions attaching to the particles, which leads to a perturbation of the ion density from fair weather values. In actual conditions, aerosols always exist, but under fair weather conditions their concentrations are small enough to not significantly affect the ionic content of the atmosphere. Therefore, for the modelling purposes of fair weather conditions, aerosol concentrations can be neglected. ~~Under fair weather atmospheric conditions, complete lack of particles in the atmospheric circulation is expected, except of ions.~~ In the steady state of such an atmosphere, the divergence of the total current is zero $\vec{\nabla} \vec{J}_{tot} = 0$, as a direct consequence of the continuity equation and hence the conduction current remains constant with altitude. From Ohm's law, we can relate the conduction current, J_z, with the vertical component of the electric field, E_z (Fig. 3a), as:

$$J_z = \sigma E_z \quad (3)$$

where σ is the atmospheric conductivity and assume a smooth conductivity profile along the altitude z, as:

$$\sigma = \sigma_0 \, exp\left(\frac{z}{l}\right) \quad (4)$$

Formatted: Font: Bold, No underline

Formatted: Indent: Left: 0", Hanging: 0.31", Outline numbered + Level: 3 + Numbering Style: 1, 2, 3, … + Start at: 1 + Alignment: Left + Aligned at: 0.25" + Indent at: 0.75"

Formatted: No underline

Formatted: Indent: Left: 0", Outline numbered + Level: 2 + Numbering Style: 1, 2, 3, … + Start at: 1 + Alignment: Left + Aligned at: 0.25" + Indent at: 0.5"

Formatted: Indent: Left: 0.36"

Formatted: Indent: Left: 0.31"

for σ_0 and l the constants that represent the near ground atmospheric conductivity and the atmospheric scale height, respectively. The given mathematical formalism of the atmospheric conductivity is adopted also by Ilin et al. (2020). The authors demonstrated that such a profile adequately describes the main aspects of the real conductivity distribution, and can be seen as a global mean conductivity profile.

We, then, express the conduction current at ground level, J_{z_0}, as a function of the columnar resistance R_c and the potential difference $\Delta V = V_{ion} - V_0$ (5), ~~where V_{ion} is the ionospheric potential at the altitude H, and V_0 is the potential at the Earth's surface which is considered a good conductor due to soil particles that are usually covered by a thin, conducting film of water (Kanagy and Mann, 1994), hence V_0 is set equal to zero. Therefore~~therefore:

$$J_{z_0} = \frac{\Delta V}{R_c} = \frac{V_{ion}}{R_c} \tag{5}$$

where V_{ion} is the ionospheric potential at the altitude H, and V_0 is the potential at the Earth's surface which is considered a good conductor due to soil particles that are usually covered by a thin, conducting film of water (Kanagy and Mann, 1994), hence V_0 is set equal to zero.

The columnar resistance can be calculated from the conductivity profile of equation (4) (Rycroft et al., 2008), hence:

$$R_c = \int_0^H \frac{dz}{\sigma} = \frac{l}{\sigma_0}\left(1 - exp\left(-\frac{H}{l}\right)\right) \tag{6}$$

Formatted: Indent: Left: 0.31"

By combining equations (3), (5) and (6), the fair weather electric field at ground level, E_{z_0}, is of the form (Gringel et al. 1986):

$$E_{z_0} = \frac{V_{ion}}{\sigma_0 R_c} = \frac{V_{ion}}{l\left(1 - exp\left(-\frac{H}{l}\right)\right)} \tag{7}$$

which depends solely on the scale height l and the ionospheric potential V_{ion}.

However, the presence of aerosols in the atmosphere and consequently dust particles, affects atmospheric conductivity (Harrison, 2003; Siingh et al., 2007; Tinsley and Zhou, 2006; Zhou and Tinsley, 2007). Aerosols tend to scavenge atmospheric ions due to electrostatic interactions and ion thermal diffusion, leading to a reduction of the atmospheric ion density, and consequently of the atmospheric electrical conductivity. The process of ion attachment to aerosols has been exhaustively investigated in the past literature. A review paper by Long and Yao (2010) contains a summary of all models and theories regarding the aerosol charging by ions. ~~of dust particles in the atmosphere affects atmospheric conductivity. Neutral aerosols, such as uncharged dust particles, tend to scavenge smaller ions which in turn favours the production of larger ions in expense to the smaller ones (Fuchs, 1963). Since larger ions are less electrically mobile, this attachment process decreases the atmospheric conductivity.~~ The case of a steady state atmospheric desert dust layer that does not exhibit charge stratification is examined below. The layer acts as a passive electrical element (resistor), and reduces the fair weather atmospheric conductivity due to the ion attachment to dust particles, by a varying reduction factor n. Fig. 3b, represents the above layer configuration, where the new conductivity profile within the layer along the altitude z, will be:

$$\sigma' = \frac{\sigma_0}{n} exp\left(\frac{z}{l}\right) \tag{8}$$

The electric field at ground due to the dust layer, $E_{z_0,layer}$, is given by:

$$E_{z_0,layer} = \frac{V_{ion}}{\sigma_0 R_c{}'} \tag{9}$$

with the new columnar resistance, $R_c{}'$, being:

$$R_c{}' = \int_0^{z_1} \frac{dz}{\sigma} + \int_{z_1}^{z_1} \frac{dz}{\sigma'} + \int_{z_1}^{H} \frac{dz}{\sigma}, \qquad z \neq z_{1,2} \quad \Rightarrow$$

$$R_c{}' = \frac{l}{\sigma_0}\left[1 + (n-1)exp\left(-\frac{z_c - d/2}{l}\right)\left(1 - exp\left(-\frac{d}{l}\right)\right) - exp\left(-\frac{H}{l}\right)\right] \tag{10}$$

where $z_{1,2}$ are the layer bottom/top heights, z_c is the mean layer central height, and $d = z_2 - z_1$ is the mean layer depth. The dust layer horizontal extent R (radius), as depicted in Fig. 3b, is assumed to be at least ten times larger than its vertical extent ($R \geq 10d$) for a thin layer approximation.

And (9) gives through (10):

$$E_{z_0,layer} = \frac{V_{ion}}{l\left[1 + (n-1)exp\left(-\frac{z_c - d/2}{l}\right)\left(1 - exp\left(-\frac{d}{l}\right)\right) - exp\left(-\frac{H}{l}\right)\right]} \tag{11}$$

~~where $z_{1,2}$ are the layer bottom/top heights, z_c is the mean layer central height, d is the mean layer depth and R is the layer horizontal extent (radius) which is assumed to be at least ten times larger than its vertical extent ($R \geq 10d$).~~ Therefore, it is clear that $E_{z_0,layer}$ depends on the scale height parameter l, the reduction parameter n, the layer central height z_c and the layer depth d ~~$= z_2 - z_1$.~~ A further investigation of the E-field dependence on the various parameters listed above can be found in the Appendix A.

~~This dependence is further investigated in Section 3.3.1.~~

On a next step, we parameterize an electrically active dust layer to calculate its impact on the surface E-field. Specifically, we construct a simplistic model for the atmospheric column (1D), based on the hypothesis that the charge accumulation areas within the dust layer can be approximated by charged cylinders of a total charge density $\pm\rho$ (Fig. 3c). For the cylinder, we assume that its horizontal extent, as represented by the cylinder radius R_1 in Fig. 3c, is at least ten times larger than the vertical extent (large cloud approximation), to ensure that the field lines are vertical with only weak radial dependence directly below the center of the layer (e.g., Riousset et al., 2007).~~10 times larger than the vertical extent, to simulate horizontally homogeneous charge distributions.~~ The electric field of such an idealized finite extent charged layer is dependent on the distance from the layer~~, with the field lines having only weak radial dependence directly below the center of the layer~~. Departures from this behaviour occur near layer edges and distances comparable to the layer extent. Moreover, ~~T~~the hypothesis of the presence of image charges is also applied due to the ground being a good conductor, ensuring that the calculated electric potentials are solutions to the Poisson equation.

The formulation for such an electrically active layer consists of a superposition of the electrically neutral dust layer case with the monopole charged cylinder case, constrained for zero ground and zero ionospheric potentials. The derivation of the ground

Formatted Table

Formatted: Indent: Left: 0.31"

Formatted: Not Highlight

Formatted: Greek

electric field due to the presence of a total charge density of ρ is given below. We calculate the potential at point A (central lower point of the charged cylinder), as specified in Fig. 3c, which is given as the sum of the potential ~~from~~from the total charge Q and the potential from its image charge Q_{img}, where $Q_{img} = -Q$:

$$V_A = V_Q + V_{Q_{img}} \tag{12}$$

The solution for the potential at the central axis of a solid charged cylinder with total charge density ρ_1, is given by (e.g., Griffiths Instructor's Solution Manual for Introduction to Electrodynamics, 4th Edition, 2013):~~(e.g. Griffiths Instructor's Solutions Manual):~~

$$V_Q = \frac{\rho_1}{4\varepsilon_0}\left\{ d_1\sqrt{{R_1}^2 + {d_1}^2} + {R_1}^2 \ln\left[\frac{d_1 + \sqrt{{R_1}^2 + {d_1}^2}}{R_1}\right] - {d_1}^2 \right\}, \qquad for\ R_1 \geq 10 d_1 \tag{13}$$

where ε_0 is the permittivity of vacuum, R_1 the charge region horizontal extent presented by the cylinder radius, $d_1 = z_2{}' - z_1{}'$ the cylinder depth (charge region vertical extent) and ρ_1 is the total charge density. Correspondingly, the potential at point A due to the image charge is calculated as:

$$V_{Q_{img}} = \frac{-\rho_1}{4\varepsilon_0}\left\{ 2z_{c_1}\sqrt{{R_1}^2 + \left(2z_{c_1}\right)^2} - \left(2z_{c_1} - d_1\right)\sqrt{{R_1}^2 + \left(2z_{c_1} - d_1\right)^2} + {R_1}^2 \ln\left[\frac{2z_{c_1} + \sqrt{{R_1}^2 + \left(2z_{c_1}\right)^2}}{\left(2z_{c_1} - d_1\right) + \sqrt{{R_1}^2 + \left(2z_{c_1} - d_1\right)^2}}\right] - 2d_1\left(2z_{c_1} - \frac{d_1}{2}\right)\right\} \tag{14}$$

for z_{c_1} the charged area central height. The new columnar resistance up to the height of point A, will be:

$$R_{c_1} = \int_0^{z_1} \frac{dz}{\sigma} + \int_{z_1}^{z_1{}'} \frac{dz}{\sigma'} \Rightarrow$$

$$R_{c_1} = \frac{l}{\sigma_0}\left[1 - exp\left(-\frac{z_c - d/2}{l}\right)\right] + \frac{nl}{\sigma_0}\left[exp\left(-\frac{z_c - d/2}{l}\right) - exp\left(-\frac{z_{c_1} - d_1/2}{l}\right)\right] \tag{15}$$

calculated from the ground to the dust layer bottom height z_1, and from there to the cylindrical charged area bottom height $z_1{}'$ (Fig. 3c). Note that d is the layer depth while d_1 is the cylinder depth.

And again, from Ohm's law and equation (15), we get the electric field at ground level for the case of a charged cylindrical monopole as:

$$E_{z_0,Q} = \frac{V_A}{l\left[1 - exp\left(-\frac{z_c - d/2}{l}\right)\right] + nl\left[exp\left(-\frac{z_c - d/2}{l}\right) - exp\left(-\frac{z_{c_1} - d_1/2}{l}\right)\right]} \tag{16}$$

where V_A is given from equations (12) to (14), with $E_{z_0,Q}$ being dependent on the scale height l, the conductivity reduction factor n, the central layer height z_c and the charged area central height z_{c_1}.

Formatted: Indent: Left: 0.31"

Formatted: Indent: Left: 0.38"

Formatted: Font: Italic

In the case of multiple stratified charged areas within the layer, the electric field at ground level is a superposition of the contribution to the field from each charge and its image (E_{z_0,Q_i}), along with the non-stratified dust layer's contribution attributed to the imposed conductivity reduction ($E_{z_0,layer}$), hence:

$$E_{z_0,multipole} = \sum E_{z_0,Q_i} + E_{z_0,layer} \Rightarrow$$
$$E_{z_0,dipole} = E_{z_0,\text{lower cylinder}} + E_{z_0,\text{upper cylinder}} + E_{z_0,layer} \quad (17)$$

where, subsequently, if we assume a dipole charge configuration within the dust layer, the total contribution to the ground E-field ($E_{z_0,dipole}$) will be a superposition of the influence from the lower ($E_{z_0,\text{lower cylinder}}$) and upper ($E_{z_0,\text{upper cylinder}}$) charged areas, along with the electrically neutral dust layer's contribution ($E_{z_0,layer}$).

3 Model outputs~~Results~~

As a result of the mathematical formalism described in Section 2.3, we present the 1D model outputs and restrictions under which the various behaviours of the near-ground E-field strength can be exhibited in comparison to the calculated fair weather E-field. ~~In order to explain the observed electrical behaviour, we examine the ground E-field effect of electrically neutral dust at first and thereafter calculate the E-field strength following the formalism for a charge stratified dust layer (see Section 2.3). Then, we compare it with the E-field values under local fair-weather conditions for selected atmospheric electric parameters.~~ Following this formulation, the dust layer that exhibits charge separation is approximated with a dipole of oppositely charged cylinders. The influence of small charge imbalances, less than 10%, in the bipolar case, which could quantitatively explain the enhancement or reduction in the E-field is also investigated. If multiple charge accumulation regions are suspected within the dust layer (Zhang and Zhou, 2020), the problem can be still represented by the model output through a superposition of several cylindrical monopoles with different charge densities, polarities and separation distances. ~~In section 3.3.3 we also investigate the influence of small charge imbalances (less than 10%) in the bipolar case, which could quantitatively explain the enhancement and reduction in the E-field.~~

3.1 ~~3.3~~ E-field below Fair weather field~~Modelled E-field below the LREF~~

In this section, we describe the possible cases under which lofted dust layers can reduce the near-ground E-~~electric~~-field strength below the reference electric field values, and we investigate whether electrified dust layers can reproduce such a behaviour. $E_{z_0,layer}$ dependency on the various atmospheric parameters points to atmospheric conductivity as the dominant factor that affects the E-field (see Appendix A). Therefore, we expect that if the dust layer is electrically neutral and acts as a passive element by reducing the atmospheric conductivity, it will greatly affect the field by forcing it below the local reference values.

Since there is little data on vertical~~the~~ profiling of the dust layer ~~the~~ electrical properties ~~of elevated dust layers and, to this point, there is no clear depiction of the potential charge accumulations areas~~, we use the previous measurements of electric

Formatted: Indent: Left: 0.31"

Formatted: Normal, No bullets or numbering

Formatted: Indent: Left: 0", Hanging: 0.13", Outline numbered + Level: 1 + Numbering Style: 1, 2, 3, … + Start at: 1 + Alignment: Left + Aligned at: 0.25" + Indent at: 0.5"

Formatted: Indent: Left: 0", Outline numbered + Level: 2 + Numbering Style: 1, 2, 3, … + Start at: 1 + Alignment: Left + Aligned at: 0.25" + Indent at: 0.5"

Formatted: Greek

field ~~change~~ variation with altitude, which indicated a charge density of $\rho = \pm 25$ pC/m^3 within a transported Saharan dust layer away from the emission source (Nicoll et al., 2011). From the specific value, the total charge Q is estimated for the different model cylinder extents. Gringel and Muhleisen (1978) measured a reduction of the electrical conductivity, compared to the fair weather values, by a factor of four within an elevated dust layer and we, therefore, adopt a reduction factor of $n = 4$ in the present study (see also Appendix A). For ~~In order to calculate~~ E_{z_0}, $E_{z_0,layer}$ and $E_{z_0,Q}$ estimations, the scale height is fixed to a globally average value of $l = 6$ km (Kalinin et al., 2014; Stolzenburg and Marshall, 2008), the ionospheric potential is fixed at $V_{ion} = 250$ kV and the ionospheric height is at $H = 70$ km. The mean central height of the dust layer and mean layer depth are both set equal to 3 km ($z_c = d = 3$ km~~$z_c = 3$ km, $d = 3$~~), since this height represents the average value for the four dust cases according to the lidar ~~V~~PLDR profiles (Table 1).

3.1.1 Balanced/Imbalanced dipole field below Fair weather field

We consider the case of two oppositely charged cylinders with similar geometries as in Fig. 3c, assuming they are within a dust layer with a mean height of 3 km and a mean depth of 3 km. The lower cylinder central height z_{c_1} starts at 2.95 km and decreases, the upper cylinder central height z_{c_2} starts also at 2.95 km for zero separation distance (at this limit, it represents electrically neutral dust that lacks internal E-field generation due to the absence of charge separation) and increases within the dust layer boundaries (varying separation distance), while their depth is fixed at 100 m~~.~~, in order to be of finite vertical extend but quite thin. The separation distance between the two cylinders is defined as the difference between their central heights and the ground E-field is a superposition of the electric field of the upper and lower cylinders. We assume the bottom cylinder to be positively charged with density $+\rho$ and the upper one to be negatively charged with $-\rho$ (Fig. 4a), in order to simulate gravitational settling conditions for larger and, most probably, positively charged dust particles (Forward et al., 2009; Waitukaitis et al., 2014).

From equations (12) to (17), the field is analytically calculated directly on the axis of the charged cylinders and plotted against the cylinder radius R for separation distances up to 800 m ~~(Fig. 9)~~. As seen in Fig. 4~~Fig. 9~~, the resulting electric field values on ground level are consistently below the fair weather constant value. When the dipole separation distance increases, the vertical electric field at ground level increases~~, but when kept relatively small (Fig. 9), the E-field increases but not sufficiently to overcome the LREF~~. This happens due to the stronger influence of the lower charged cylindrical layer to the surface resistance. ~~the fact that as~~ The fact that the upper charged ~~layer~~cylinder moves to higher altitudes signifies that~~,~~ the resistance between the specific layer and the ground increases, therefore the conduction current at the ground decreases. ~~Hence, t~~The conduction current due to the upper charged layer, ~~is~~then, becomes weaker than the conduction current due to the lower charged layer, which moves towards the ground. Since the conductivity at the ground is undisturbed by the dust layer (Fig. 3c) and equal to the fair weather value, the ground electric field due to the upper layer decreases as the layer moves up, while the field due to the lower layer increases as the layer approaches the ground, leading to an increasing value of the total electric field with the increasing separation distance. When the separation distance is kept relatively small, the enhancement effect in the E-field is not significant enough to overcome the fair weather values (Fig. 4).

Formatted: Indent: Left: 0", Hanging: 0.31", Outline numbered + Level: 3 + Numbering Style: 1, 2, 3, … + Start at: 1 + Alignment: Left + Aligned at: 0.25" + Indent at: 0.75"

Formatted: Font: Bold, No underline

~~For~~For large radii, although the infinite plates configuration is asymptotically approached ($E_{z_o,dipole} \rightarrow 0$), there is a nearly-constant residual field for the finite cylindrical geometry of the charged regions. Since the charged cylinders are placed in a conducting medium above a perfect conductor, the electric field at the ground will not be zero even if the cylinders have infinite extent. Due to the conductivity distribution, there is an uneven contribution of the electric fields of each cylinder and, therefore, the E-field is expected to converge to this non-zero value (Fig. 4~~Fig. 9~~).

~~3.3.3 Imbalanced charged dipole field below the LREF~~

If ~~we assume that~~ the dipole charge density is not uniformly distributed to both cylinders, ~~leading~~resulting in~~to~~ a charge imbalance within the layer, ~~we expect that~~ the electric field will be more sensitive to separation distance changes (Fig. 4b). Such imbalance could be the result of (a) dust charging at the source, prior to any charge separation that may occur (Ette, 1971; Kamra, 1972), (b) charging due to atmospheric current, or (c) charge loss through dry deposition in the Planetary Boundary Layer (PBL). ~~The latter effect may occur when the base dust layer descends into the PBL, as in the case of the June 23rd dust layer.~~ In Fig. 5~~Fig. 10~~, the ground electric field dependence on the separation distance and cylinder radius is depicted, for a charge density difference of $\Delta\rho = 2$ pC/m^3 (8%) between the two charged cylindrical areas, with the upper one being less charged. This leads to a larger increase of the E-field than in the balanced dipole case (Fig. 4a), as the effect of the upper cylinder not only decreases as it moves to higher altitudes, but it is also reduced due to the reduction of the total charge density which influences proportionally the electric field. Note that even a small imbalance can highly increase the external field. Nevertheless, for relatively small separation distances the resulting field values fall again below the fair weather value. ~~Nevertheless, for relatively small separation distances the resulting field values fall below the LREF values. Therefore, considering an electrically active dust layer that exhibits charge imbalance of less than 10%, can be adequate to interpret the observed reduction of the E-field below the LREF. Note that even a small imbalance can highly increase the external field.~~

3.2 E-field above Fair weather field~~3.4 Modelled E-field above the LREF~~

We examine the physical arrangement within the dust layer that can provide an enhancement to the electric field above the ~~local reference~~fair weather ~~field~~ values and subsequently above the LREF. ~~, as is the case for the dust outbreaks in the 25th of July and 20th of October.~~

3.2.1 ~~3.4.1 Balanced~~ /Imbalanced dipole field above Fair weather field~~charge dipole field above the LREF~~

For the same charged region geometries as ~~in the previous section~~discussed previously, ~~we impose~~ larger separation distances are imposed for the balanced dipole case (Fig. 5a), but we strictly remain within the base dust layer mean dimensions. Fig. 5~~Fig. 11~~ shows that as the separation distance between the oppositely charged layers increases, an enhancement of the E-field above the local reference values occurs. This enhancement becomes more prominent as the layers grow further apart within the dust plume and the contribution from the lower layer is significantly larger than the upper layer. The above dependence of the ground E-field on the separation distance is not expected in the case of charged infinite plates, as discussed in S~~s~~ection

Formatted: Normal

Formatted: Indent: Left: 0", Outline numbered + Level: 2 + Numbering Style: 1, 2, 3, … + Start at: 1 + Alignment: Left + Aligned at: 0.25" + Indent at: 0.5"

Formatted: Font: Bold, No underline

Formatted: Indent: Left: 0", Hanging: 0.31", Outline numbered + Level: 3 + Numbering Style: 1, 2, 3, … + Start at: 1 + Alignment: Left + Aligned at: 0.25" + Indent at: 0.75"

3.1.1.~~3.3.2. Since the charged cylinders are placed in a conducting medium above a conducting plane, the electric field at the ground is not expected to be zero even if the cylinders have infinite extent. The reason is that at each point of the domain, because of the conductivity distribution, there is an uneven contribution of the electric fields of each cylinder. Therefore, it is expected at infinite radii of the cylindrical formalism that the field converges to a non-zero value (residual field).~~

~~3.4.2 Imbalanced charged dipole field above the LREF~~

Again, for a charge imbalance of 8% between the two cylinders and for larger separation distances, the E-field is significantly enhanced and exceeds the local fair weather values (Fig. 5b~~Fig. 12~~). The term large or small separation distance depends on the conductivity distribution and more specifically on the conductivity scale height, as can be seen in equations (11) and (16). This increase becomes more prominent as the separation distance increases and the lower positive cylinder moves closer to the ~~field mill~~sensor location.

~~We also observe that the external E-field is more sensitive to charge imbalance, even a small one, than to separation distance variations, hence when the imbalance is larger than 8% the E-field will exceed the LREF for even smaller separation distances than the ones presented here.~~

4 Experimental Results

~~In this section, t~~The near ground electric field measurements with co-located lidar observations are presented for the four case studies of elevated Saharan dust layers, over the two atmospheric remote sensing stations. The transient dust events recorded by Polly^{XT} were, simultaneously, electrically monitored throughout the day with the field mill. According to the effect over the E-field timeseries, the dust outbreaks examined ~~here~~ are separated into two classes, the ones that effectuate an enhancement to the ground electric field and those inducing a reduction with respect to the local reference field. Through these observations, we attempt to provide evidence of electrically active dust only by ground-based methods, supported by the model configuration described in the previous sections.

4.1 Layer characterization through Polly$_{XT}$

The July 2017 and March 2018 dust events in Finokalia are characterized by large concentrations of airborne dust particles from the middle of the day onwards, followed by dust settling towards the ground after 21:00 (UTC), as indicated by the time-height plots of the total attenuated backscatter coefficient ~~with low near surface concentrations of both dust and marine aerosols, followed by advection towards the ground after 21:00 UTC~~ (~~Fig. 4~~ Fig. 6 and ~~Fig. 6~~Fig. 8). Larger particle concentrations are shown in red tones, with the β and δ_p (black lines) profiles superimposed to the respective attenuated backscatter coefficient (top panel) and δ_v (lower panel) quick-looks. For the first case study (Fig. 6), beta values are between 3 to 4 ($Mm^{-1}sr^{-1}$) with a maximum value of 5 ($Mm^{-1}sr^{-1}$) inside the layer and denote large particle concentrations. High δ_v values (> 10%) are indicative of dust particles and δ_p values between ~ 25% - 30% in the afternoon are characteristic of pure dust. Settling of dust particles below 2 km, inside the Marine Boundary Layer (MABL) is revealed from the time-height evolution

Formatted: Normal

Formatted: Indent: Left: 0", Hanging: 0.13", Outline numbered + Level: 1 + Numbering Style: 1, 2, 3, … + Start at: 1 + Alignment: Left + Aligned at: 0.25" + Indent at: 0.5"

Formatted: Not Superscript/ Subscript

Formatted: Heading 2, Indent: Left: 0", Outline numbered + Level: 2 + Numbering Style: 1, 2, 3, … + Start at: 1 + Alignment: Left + Aligned at: 0.25" + Indent at: 0.5"

of the VLDR (see Fig. 6). For the March 2018 case study (Fig. **8**), the elevated layer (small dust concentration was present near the surface) reached Finokalia at early noon. The layer was directly transported from Sahara and reached the station in less than 48 hours, as indicated by the backward trajectories analysis (Fig. 1c). Examination of the β profile in Fig. 8, shows values that reach up to 15 ($Mm^{-1}sr^{-1}$) at the top of the layer, indicating higher aerosol concentrations in this case. δ_v values close to 30% are indicative of high dust particle concentration and δ_p values persistently of 30% are characteristic of pure dust within the entirety of the layer (1 to 4 km), with dust downward mixing inside the MABL being less prominent.

~~In the areas of large total attenuated backscatter, high concentrations are expected and the VLDR values vary from 25% - 35% for both cases, which indicates pure dust areas intermingled with mixed dust. The October 2018 Antikythera layer (Fig. 5), exhibits dust particle concentrations from 2 to 5 km in altitude, mostly mixed with some low marine aerosol concentrations (Fig. 1b). The June 2019 dust outbreak consists primarily of high elevated dust concentrations (Fig. 1d), after mid-day, with pure dust VLDR values reaching up to 40% (Fig. 7), while aerosol concentrations within the Planetary Boundary Layer (PBL) are present but the dust load remains dominant between 2 km and 5 km.~~

The October 20th 2018 Antikythera layer (Fig. 7), exhibits lower dust particle concentrations (β lower than 5 $Mm^{-1}sr^{-1}$) close to the ground up to 6 km in altitude, mostly mixed with marine aerosols below 2 km (Fig. 1b and Fig. 7). High δ_v values (> 20%) are indicative of dust particle presence and δ_p between 25% - 30% in the afternoon is characteristic of pure dust. It is also observed that the near-ground dust concentration is very low, with the thin layer at 500 m being a mixture of dust particles and particles of marine origin with the VLDR around 15%. The June 23rd 2019 dust outbreak consists primarily of high elevated dust concentrations, since δ_v values are greater than 15% (Fig. 9), after mid-day, with δ_p values reaching up to 30% in the height range of 3 to 5 km, which are representative of pure dust (Fig. 9). The dust plume was transported again directly from Sahara to Antikythera within 48 hours (Fig. 1d) and very low concentrations of dust particles are also present within the MABL.

4.2 Local mean E-field behaviour

Considering the electrical properties of the layers detected in Finokalia~~As seen in (Fig. 4~~ Fig. 6 and ~~Fig. 6~~Fig. 8), ~~where~~ the LREF and the reconstructed mean electric field are depicted ~~in Finokalia~~, with the local diurnal variation ~~resembles~~ resembling the Carnegie curve. The E_z values vary between a total minimum at ~ 05:00 (UTC) and the maximum at ~ 13:00 (UTC) with a mean value of ~ 173 V/m. An increase of the electric field is observed at about 22:00 (UTC) resulting in a double peak variations curve (Yaniv et al., 2016). The reconstructed mean E-field is close to the expected fair weather value and the slight difference can be attributed to local meteorological factors, atmospheric boundary layer characteristics (Anisimov et al., 2017) and the station's coastal location. Complementarily, E_z diurnal variation in the station of Antikythera exhibits a minimum in early morning hours at ~ 23:00 (UTC) and a single maximum on early afternoon at ~ 19:00 (UTC) (Fig. 7~~Fig. 5~~ and Fig. 9~~Fig. 7~~), with a mean value of ~ 102 V/m. Since the timeseries in Antikythera are restricted to one year, the mean E-field~~E_z~~ value is statistically biased, therefore it is lower than the expected fair weather value.

Formatted: Heading 2, Indent: Left: 0", Outline numbered + Level: 2 + Numbering Style: 1, 2, 3, … + Start at: 1 + Alignment: Left + Aligned at: 0.25" + Indent at: 0.5"

~~According to the effect over the E-field timeseries, the dust outbreaks examined here are separated into two classes, the ones that effectuate an enhancement to the ground electric field and those inducing a reduction with respect to the local reference field.~~

4.3 Observed E-Field enhancement as compared to LREF

Formatted: Indent: Left: 0", Outline numbered + Level: 2 + Numbering Style: 1, 2, 3, … + Start at: 1 + Alignment: Left + Aligned at: 0.25" + Indent at: 0.5"

~~I~~In Fig. 6~~Fig. 4~~ and Fig. 7~~Fig. 5~~, we present ~~T~~the dust events that induced an~~cases with~~ enhanced electrical behaviour ~~at the surface are presented~~near the ground ~~in Fig. 4 and Fig. 5~~. The E-field strength measurements are averaged over 5 mins in order to be comparable with the lidar data. In the July 25th layer (~~Fig. 4~~Fig. 6), dust advection is recorded ~~during~~ since the first morning hours and areas of increased particle concentration can be spotted from early noon. The δ_p profile~~, as indicated by the total attenuated backscatter coefficient dependence from the altitude. Larger particle concentrations are shown in red tones (Fig. 4). The VLDR values for the same dust layer are also plotted on the lower panel and signify~~ signifies that the layer consists primarily of dust which descends after ~16:00 (UTC) and falls entirely below 2 km at ~18:30 (UTC~~.), The E-field measurements are averaged over 5 mins in order to be plotted against the lidar data~~ but the mean electric field (black line) remains above the reference field (red contoured line)~~,and remain consistently above the LREF,~~ showing an increase when particle density is maximized towards noon and a small drop when dust concentrations within the MA~~P~~BL becomes significant. A similar electrical behaviour was observed during the dust event of October 2018 that reached the PANGEA observatory. Large lofted particle concentrations are attributed to dust ~~according to~~ as discussed previously (Fig. 7)~~VLDR values that reach up to 30% (Fig. 5). It is also observed that the near-ground dust concentration is very low, with the thin layer at 500 m being of marine origin. For both cases, t~~The mean E_z appears enhanced as compared to the ~~reference field~~LREF, showing a further increase at ~ 21:00 (UTC) when dust deposition becomes prominent. According to the physical approximation of cylindrical charged areas (see Section 3.2), such an enhancement would be expected only when the lofted dust layer is electrically active and charge separation within the layer is prominent. From Fig. 5b, it becomes apparent that the external E-field is more sensitive to charge imbalances, even small ones, than to separation distance variations, hence a charge imbalance within these layers could drive the E-field above the fair weather values, as observed in the above cases, for even smaller charge separation distances.

4.4 Observed E-Field reduction as compared to LREF

Formatted: Indent: Left: 0", Outline numbered + Level: 2 + Numbering Style: 1, 2, 3, … + Start at: 1 + Alignment: Left + Aligned at: 0.25" + Indent at: 0.5"

Several dust load cases were detected, both in Finokalia and Antikythera, where the near-ground electric field strength exhibits a decrease when compared to the local reference field and, particularly, when high dust particle concentrations were present. In the specific study, we select the cases of March 2018 and June 2019 in terms of the similar temporal injection of dust particles, large AOD values and similar layer progression throughout the day (Fig. 8 and Fig. 9). From the δ_p profiles, we deduce that for both cases, the elevated layer between 2 and 4 km consists primarily of dust particles, while the decrease of δ_p towards the bottom of the layer is indicative of downward mixing inside the MABL, with marine particles of lower δ_ps. ~~As observed in Fig. 6, an elevated layer with no dust concentrations near the surface reached Finokalia in March 14th 2018, at~~

~~early noon. The layer was directly transported from Sahara and reached the station in less than 48 hours as indicated by the backward trajectories analysis (Fig. 1c). From the VLDR values (35% - 40%), we deduce that the layer consists mainly of pure dust which remains elevated between 1.5 and 4 km.~~ The mean E-field remains positive and well below the reference field, exhibiting an increase as dust injection initiates at ~~11~~09:00 UTC and then a decrease along the plume's progression (~~Fig. 6~~Fig. 8).

The dust plume of June 2019 instils a similar electrical behaviour to the ground E-field, as ~~was transported again directly from Sahara to Antikythera within 48 hours (Fig. 1d), while PBL particle concentrations were high over early morning hours and decreased as the elevated dust particle densities increase near noon. A daily average AOD value of 0.22 indicates that there is high concentration of aerosols throughout the day and the VLDR values attained from the lidar, peak to as high as 40% in the height of 4 km within the layer (Fig. 7).~~ the bottom of the layer~~Dust~~ seems to progressively move towards lower altitudes~~downwards~~ during late afternoon and ~~but~~ the total dust load ~~is~~ remains persistent ~~and renewed in the following day~~. ~~Moreover, the effect of the dust plume on the electric field is clearly similar to the previous case in Finokalia, where the mean field remains~~The mean E-field is positive and consistently below the reference field, exhibiting an increase close to fair weather values when particle injection begins towards noon and dust concentration is rising, but later drops further below the LREF as the layer progresses to lower altitudes. ~~positive and always below the LREF but appears to be increasing with rising dust concentrations.~~ Following the 1D model outputs for such a case (see Section 3.1.1), this observed reduction could be attributed to either electrically neutral dust aloft or to electrically active dust with the charged regions in relatively small separation distances within the layer. Under the electrically active dust case, a charge imbalance of less than 10%, can be adequate to interpret the observed reduction of the E-field below the LREF for even smaller separation distances. But the detection of such an E-field reduction below the LREF cannot conclusively characterize the electrical activity of the dust layer aloft.

4.5 ~~3.5~~ Reversed E-field polarity

If a reversed polarity E-field is observed (in our timeseries there were dust cases under which the field exhibited polarity reversal), with the opposite sign signifying that the field vector points upwards instead of downwards, then the investigated formalism is capable of explaining the reversal. As such, a similar cylindrical configuration ~~is~~could be assumed with the only difference being that the lower layer has to be negatively charged and the upper one, in the dipole case, to be positively charged. Under this condition, the conclusions ~~in Fig. 9 to Fig. 12~~derived from the model remain the same. Therefore, such an indication of reversal is explained only via reversed separated cylindrical charges and again points that lofted dust has to be electrified.

Formatted: Indent: Left: 0", Outline numbered + Level: 2 + Numbering Style: 1, 2, 3, … + Start at: 1 + Alignment: Left + Aligned at: 0.25" + Indent at: 0.5"

~~Through observations of the electric field during the dust outbreaks reported above, we can attempt to provide evidence of electrically active dust by ground-based methods. In order to explain the observed electrical behaviour, we examine the ground E-field effect of electrically neutral dust at first and thereafter calculate the E-field strength following the formalism for a charge-stratified dust layer (see Section 2.3). Then, we compare it with the E-field values under local fair-weather conditions~~

for selected atmospheric electric parameters. Following this formulation, the dust layer that exhibits charge separation is approximated with a dipole of oppositely charged cylinders. If multiple charge accumulation regions are suspected, the problem can be represented by a superposition of several cylindrical monopoles with different charge densities, polarities and separation distances. In section 3.3.3 we also investigate the influence of small charge imbalances (less than 10%) in the bipolar case, which could quantitatively explain the enhancement and reduction in the E-field.

3.3 Modelled E-field below the LREF

In this section, we describe the possible cases under which lofted dust layers can reduce the near-ground electric field strength below the reference electric field values, and investigate whether electrified dust layers can reproduce such a behaviour. Since there is little data on the profiling of the electrical properties of elevated dust layers and, to this point, there is no clear depiction of the potential charge accumulations areas, we use the previous measurements of electric field change with altitude, which indicated a charge density of $\rho = \pm 25$ pC/m^3 within a transported Saharan dust layer away from the emission source (Nicoll et al., 2011). From the specific value, the total charge Q is estimated for the different model cylinder extents. In order to calculate E_{z_g}, $E_{z_g,layer}$ and $E_{z_g,Q}$, the scale height is fixed to a globally average value of $l = 6$ km (Kalinin et al., 2014; Stolzenburg and Marshall, 2008), the ionospheric potential is fixed at $V_{ion} = 250$ kV and the ionospheric height is at $H = 70$ km. The mean central height of the dust layer and mean layer depth are both set equal to 3 km ($z_c = 3$ km, $d = 3$), since this height represents the average value for the four dust cases according to the lidar VLDR profiles (Table 1).

3.3.1 Dust layer acting as a passive element

In Fig. 8., the dependence of $E_{z_g,layer}$ (red line) on the conductivity reduction factor, the scale height, the layer central height and the layer depth, as given in (11), is plotted and compared to the fair weather electric field E_{z_g} at ground (blue line) which is given by (7). E_{z_g} depends only on the scale height and decreases as l increases, while it remains constant for the other varying parameters as expected from equation (7). The calculated fair weather field value of ~ 42 V/m, for the selected l, is comparable to the estimated value by Williams (2003) from Ohm's law, when dividing the globally integrated conduction current density by the mean atmospheric electrical conductivity at ground ($J_{z_g} \approx 2x10^{-12} A/m^2, \sigma_a \approx 5x10^{-14} S/m$) and assuming an exponentially increasing conductivity profile above the Earth's surface (Haldoupis et al., 2017). We note that this globally average value of E_{z_g} is much less from the typically measured which is around 100 V/m (e.g. Corney et al., 2003; Reddell et al., 2004). We believe that the average value is more suitable for global calculations, because it incorporates the variations of the conductivity distribution around the Earth. On the other hand, the typical value is tied to the location of the measurement, and it varies at different locations as the conductivity distribution changes.

Consequently, $E_{z_g,layer}$ exhibits the greatest variation with the reduction factor n, meaning that atmospheric conductivity reduction is the predominant factor that affects the E-field strength by largely lowering it. Therefore, we expect that if the dust layer is electrically neutral, it reduces the atmospheric conductivity and affects the ground electric field by forcing it below the

local reference values. Gringel and Muhleisen (1978) measured a reduction of the electrical conductivity, compared to the fair weather values, by a factor of four within an elevated dust layer, while an increase of the electric field within an Alpine peak layer by a factor of two has also been observed (Reiter, 1992). We, therefore, adopt a reduction factor of $n = 4$ in the present study.

3.3.2 Balanced charged dipole field below the LREF

We consider the case of two oppositely charged cylinders with similar geometries as in Fig. 3c, assuming they are within a dust layer with a mean height of 3 km and a mean depth of 3 km. The lower cylinder central height z_{c_-} starts at 2.95 km and decreases, the upper cylinder central height z_{c_+} starts also at 2.95 km for zero separation distance (at this limit, it represents electrically neutral dust that lacks internal E-field generation due to the absence of charge separation) and increases within the dust layer boundaries (varying separation distance), while their depth is fixed at 100 m. The separation distance between the two cylinders is defined as the difference between their central heights and the ground E-field is a superposition of the electric field of the upper and lower cylinders. We assume the bottom cylinder to be positively charged with density $+\rho$ and the upper one to be negatively charged with $-\rho$, in order to simulate gravitational settling conditions for larger and, most probably, positively charged dust particles (Forward et al., 2009; Waitukaitis et al., 2014).

From equations (12) to (17), the field is analytically calculated directly on the axis of the charged cylinders and plotted against the cylinder radius R for separation distances up to 800 m (Fig. 9). As seen in Fig. 9, the resulting electric field values on ground level are consistently below the fair weather constant value. When the dipole separation distance increases, the vertical electric field at ground level increases, but when kept relatively small (Fig. 9), the E-field increases but not sufficiently to overcome the LREF. This happens due to the fact that as the upper charged layer moves to higher altitudes, the resistance between the layer and the ground increases, therefore the conduction current at the ground decreases. Hence, the conduction current due to the upper charged layer is weaker than the conduction current due to the lower charged layer, which moves towards the ground. Since the conductivity at the ground is undisturbed by the layer and equal to the fair weather value, the ground electric field due to the upper layer decreases as the layer moves up, while the field due to the lower layer increases as the layer approaches the ground, leading to an increasing value of the total electric field with the increasing separation distance. For large radii, although the infinite plates configuration is asymptotically approached ($E_{z_c,dipole} \to 0$), there is a nearly-constant residual field for the finite cylindrical geometry of the charged regions. Since the charged cylinders are placed in a conducting medium above a perfect conductor, the electric field at the ground will not be zero even if the cylinders have infinite extent. Due to the conductivity distribution, there is an uneven contribution of the electric fields of each cylinder and, therefore, the E-field is expected to converge to this non-zero value (Fig. 9).

3.3.3 Imbalanced charged dipole field below the LREF

If we assume that the dipole charge density is not uniformly distributed to both cylinders, leading to a charge imbalance within the layer, we expect that the electric field will be more sensitive to separation distance changes. Such imbalance could be the

result of (a) dust charging at the source, prior to any charge separation that may occur (Ette, 1971; Kamra, 1972), (b) charging due to atmospheric current, or (c) charge loss through dry deposition in the PBL. The latter effect may occur when the base dust layer descends into the PBL, as in the case of the June 23rd dust layer. In Fig. 10, the ground electric field dependence on the separation distance and cylinder radius is depicted, for a charge density difference of $\Delta\rho = 2$ pC/m^3 between the two charged cylindrical areas, with the upper one being less charged. This leads to a larger increase of the E-field than in the balanced dipole case, as the effect of the upper cylinder not only decreases as it moves to higher altitudes, but it is also reduced due to the reduction of the total charge density which influences proportionally the electric field. Nevertheless, for relatively small separation distances the resulting field values fall below the LREF values. Therefore, considering an electrically active dust layer that exhibits charge imbalance of less than 10%, can be adequate to interpret the observed reduction of the E-field below the LREF. Note that even a small imbalance can highly increase the external field.

3.4 Modelled E-field above the LREF

We examine the physical arrangement within the dust layer that can provide an enhancement to the electric field above the local reference field, as is the case for the dust outbreaks in the 25th of July and 20th of October.

3.4.1 Balanced charge dipole field above the LREF

For the same charged region geometries as in the previous section, we impose larger separation distances for the balanced dipole case, but we strictly remain within the base dust layer mean dimensions. Fig. 11 shows that as the separation distance between the oppositely charged layers increases, an enhancement of the E-field above the local reference values occurs. This enhancement becomes more prominent as the layers grow further apart within the dust plume and the contribution from the lower layer is significantly larger than the upper layer. The above dependence of the ground E-field on the separation distance is not expected in the case of charged infinite plates, as discussed in section 3.3.2. Since the charged cylinders are placed in a conducting medium above a conducting plane, the electric field at the ground is not expected to be zero even if the cylinders have infinite extent. The reason is that at each point of the domain, because of the conductivity distribution, there is an uneven contribution of the electric fields of each cylinder. Therefore, it is expected at infinite radii of the cylindrical formalism that the field converges to a non-zero value (residual field).

3.4.2 Imbalanced charged dipole field above the LREF

Again, for a charge imbalance of 8% between the two cylinders and for larger separation distances, the E-field is significantly enhanced and exceeds the local fair-weather values (Fig. 12). The term large or small separation distance depends on the conductivity distribution and more specifically on the conductivity scale height, as can be seen in equations (11) and (16). This increase becomes more prominent as the separation distance increases and the lower positive cylinder moves closer to the field mill. We also observe that the external E-field is more sensitive to charge imbalance, even a small one, than to separation

distance variations, hence when the imbalance is larger than 8% the E-field will exceed the LREF for even smaller separation distances than the ones presented here.

3.4.3 E-field dependence on the bottom charged area height

From the above discussion, the question that arises is whether the proximity of the lower cylinder, to the ground itself, is capable to reproduce the electric field enhancement feature above the LREF. It becomes clear that two mechanisms act upon the enhancement of the ground electric field. The first is the decrease of the contribution of the upper layer as it moves upwards, due to the enhancement of the columnar resistance between the layer and the ground. The second is the increase of the contribution of the lower layer as it moves downwards, due to the decrease of the columnar resistance between the layer and the ground. The closer the lower layer is to the ground the smaller the separation with the upper layer is required for the enhancement of the electric field.

In order to validate the influence of each parameter, we re-examine the ground E-field behaviour by keeping the lower cylinder at a fixed altitude of 2 km (close to the dust layer base, similarly to thundercloud activity e.g. Mallios & Pasko, 2012) and we, then, increase the separation distance. As observed in Fig. 13, the increasing separation distance causes the E-field to increase at the ground and when it becomes large enough (Fig. 13, top and bottom right panels), the upper cylinder does no longer influence the ground E-field. At this point, for both balanced and imbalanced dipoles with cylinder radius larger than ~40 km, the field converges to a constant value. This becomes clearer when comparing Fig. 13 with Fig. 9. When the separation distance is 400 m, the electric field at the ground is larger than the reference field in the case of Fig. 13, while at Fig. 9, separation distance equal to 400 m happens when the bottom layer is at 2.75 km. In this case, the field is lower than the reference value which indicates that the closer the bottom layer is to the ground, the smaller the separation distance needed for the enhancement of the ground electric field above the reference field. Moreover, the E-field value for zero separation distance is consistently below the calculated fair weather value. As such, observations of enhanced E-field above the fair weather values, for dust driven days, can be reproduced only when an electrically active dust layer is transported above the fieldmill.

If we assume that the bottom charged area is close to the lofted layer base, we would expect an increase to the ground electric field as the layer progressively moves towards lower altitudes. For the comparison of the E-field timeseries with the descending layer base (Fig. 14), we use the cross component of the lidar attenuated backscatter coefficient at 532 nm, from which we can derive information on the vertical extent of the aerosol layers. More specifically, we applied a methodology where the first derivative of the attenuated backscatter coefficient is used to determine layer boundaries (Flamant et al., 1997; Mattis et al., 2008). The local maximum and local minimum of the derivative are considered to be the bottom and top of the layer respectively. The agreement between the height time displays of the attenuated backscatter coefficient and the corresponding gradient (Fig. 4 to Fig. 7and Fig. 14) can be used to verify the results of the gradient method.

As seen in the July 2017, March 2018 and June 2019 dust events, there is an enhancement of the reconstructed mean E-field followed by the layer base progression towards the ground, for specific timeframes within the day. This could signify the presence of positive charges accumulated to the layer base.

~~**3.5 Reversed E-field polarity**~~

~~If a reversed polarity E-field is observed (in our timeseries there were dust cases under which the field exhibited polarity reversal), with the opposite sign signifying that the field vector points upwards instead of downwards, then the investigated formalism is capable of explaining the reversal. As such, a similar cylindrical configuration is assumed with the only difference being that the lower layer has to be negatively charged and the upper one, in the dipole case, to be positively charged. Under this condition, the conclusions in Fig. 9 to Fig. 12 remain the same. Therefore, such an indication of reversal is explained only via reversed separated cylindrical charges and again points that lofted dust has to be electrified.~~

5 Discussion

5.1 ~~3.4.3~~ E-field dependence on the bottom charged area height

From the above ~~discussion~~results, the question that arises is whether the proximity of the lower cylinder, to the ground itself, is capable to reproduce the electric field enhancement feature above the LREF. It becomes clear that two mechanisms act upon the enhancement of the ground electric field. The first is the decrease of the contribution of the upper layer as it moves upwards, due to the enhancement of the columnar resistance between the layer and the ground. The second is the increase of the contribution of the lower layer as it moves downwards, due to the decrease of the columnar resistance between the layer and the ground. The closer the lower layer is to the ground the smaller the separation with the upper layer is required for the enhancement of the electric field.

In order to validate the influence of each parameter, we re-examine the ground E-field behaviour by keeping the lower cylinder at a fixed altitude of 2 km (close to the dust layer base, similarly to thundercloud activity e.g., ~~(~~Mallios and Pasko, 2012) and we, then, increase the separation distance. As observed in Fig. 10~~Fig. 13~~, the increasing separation distance causes the E-field to increase at the ground and when it becomes large enough (~~Fig. 13,~~ top and bottom right panels), the upper cylinder does no longer influence the ground E-field. At this point, for both balanced and imbalanced dipoles with cylinder radius larger than ~ 40 km, the field converges to a constant value. This becomes clearer when comparing Fig. 10~~Fig. 13~~ with Fig. 4~~Fig. 9~~. When the separation distance is 400 m, the electric field at the ground is larger than the reference field in the case of Fig. 10~~Fig. 13~~, while at Fig. 4~~Fig. 9~~, separation distance equal to 400 m happens when the bottom layer is at 2.75 km. In this case, the field is lower than the reference value which indicates that the closer the bottom layer is to the ground, the smaller the separation distance needed for the enhancement of the ground electric field above the reference field. Moreover, the E-field value for zero separation distance is consistently below the calculated fair weather value. As such, observations of enhanced E-field above the fair weather values, for dust driven days, can be reproduced only when an electrically active dust layer is transported above the field mill.

If we assume that the bottom charged area is close to the lofted layer base, we would expect an increase to the ground electric field as the layer progressively moves towards lower altitudes. For the comparison of the E-field timeseries with the descending layer base (Fig. 11~~Fig. 14~~), we use the cross component of the lidar attenuated backscatter coefficient at 532 nm, from which

Formatted: Indent: Left: 0", Hanging: 0.13", Outline numbered + Level: 1 + Numbering Style: 1, 2, 3, … + Start at: 1 + Alignment: Left + Aligned at: 0.25" + Indent at: 0.5"

Formatted: Font: Bold, No underline

Formatted: Heading 2, Indent: Left: 0", Outline numbered + Level: 2 + Numbering Style: 1, 2, 3, … + Start at: 1 + Alignment: Left + Aligned at: 0.25" + Indent at: 0.5"

we can derive information on the vertical extent of the aerosol layers. More specifically, we applied a methodology where the first derivative of the attenuated backscatter coefficient is used to determine layer boundaries (Flamant et al., 1997; Mattis et al., 2008). The local maximum and local minimum of the derivative are considered to be the bottom and top of the layer respectively. The agreement between the height–time displays of the attenuated backscatter coefficient and the corresponding gradient (Fig. 6~~Fig. 4~~ to Fig. 9 ~~Fig. 7~~and Fig. 11~~Fig. 14~~) can be used to verify the results of the gradient method.

As seen in the July 2017, March 2018 and June 2019 dust events, there is an enhancement of the reconstructed mean E-field followed by the layer base progression towards the ground, for specific timeframes within the day. This could signify the presence of positive charges accumulated to the layer base.

5.2 Chauvenet criterion validity

Formatted: Indent: Left: 0", Outline numbered + Level: 2 + Numbering Style: 1, 2, 3, … + Start at: 1 + Alignment: Left + Aligned at: 0.25" + Indent at: 0.5"

In ~~section~~ Section 2.2.2~~2.2.2~~, we described the processing chain for the determination of the local fair weather days at both atmospheric remote sensing stations. The novelty of the approach lies to the fact that only signal processing constraints are used, without incorporating criteria of local meteorological parameters that could redefine the initial conditions for the total fair weather days determination (Harrison and Nicoll, 2018). Nonetheless, threshold values concerning these factors are subjective, and may vary from study to study, which leads to differences in the extracted fair weather days. The specific study proposes a mathematically strict approach with the imposition of the Chauvenet criterion, which exploits only the field mill data and has a physical impact on the dataset. Under fair weather days, the mean electric field is approximately constant and the fewer by far dust driven days as captured in both stations, which are about 10% of the days within a typical year for both stations, will not influence significantly the reconstructed mean field value, but will be well beyond the standard deviation. The Chauvenet criterion excludes the days with such high variations as outliers and, therefore, the methodology for the reconstruction of the local reference field is less biased to variations occurring in dust driven days.

5.3 Generalization of the cylindrical model and LREF methodology

Formatted: Indent: Left: 0", Outline numbered + Level: 2 + Numbering Style: 1, 2, 3, … + Start at: 1 + Alignment: Left + Aligned at: 0.25" + Indent at: 0.5"

The methodology followed for the calculation of the ground electric field can be expanded to the area away from the central axis of the charged cylinders. As the cylinder radius increases and the infinite plate regime is approached, effects due to charged layer edges that induce radial electric field components, do not impact the sensor axis for a larger horizontal extent of the charged layer. This expands the analytical calculation as it becomes valid within a band region further away from the cylinder center. In the small radius regime, the sensor becomes sensitive to edge effects and the edge field can be far stronger than the on-axis field. If we assume that a transient dust layer is transported with a mean wind speed of 10 m/s, implying a regional scale transport, then in a period of 2 hrs the edge will be 72 km away from the sensor axis (fast transits), a sufficient distance to not affect the vertical component of the electric field. Although these variations are present on the raw timeseries (observed peak activity in ~~Fig. 4~~Fig. 6, ~~Fig. 6~~ Fig. 8 and ~~Fig. 7~~Fig. 9), in the reconstruction of the LREF variations with timescales shorter than 6 hrs are the lower limit to the FFT input and are therefore excluded. This leaves the LREF unbiased to edge effects. Problems might be caused in our analysis in the case of very slowly moving dust layers, that are transported with wind speeds

less than 1 m/s. Dust layer edge effects can provide basic information on the layer properties and could be incorporated in our cylindrical layer formalism, but this consists ~~it will be~~ a subject of further investigation in the near future.

6 Summary and Conclusions

Near-ground electric field strength observations during Saharan dust advection over Greece exhibit three distinct responses of enhancement, reduction or sign reversal when compared to local fair weather values. In this paper, we present four cases of transient dust events that influence the ground electric field recorded at two atmospheric remote sensing stations synergistically with a lidar system and a field mill electrometer. Moreover, this work attempts to use only ground-based atmospheric electricity instrumentation as a proxy for electrified dust detection, with characterization in terms of optical properties from lidar observations. To quantify the effect of charged dust particles, we implemented a reference electric field representing the local fair weather field, using long-term measured timeseries, and examine the possible physical mechanisms that could explain the electric field behaviour. Our findings suggest that dust cases with the reconstructed mean E-field magnitude above the reference field indicate charge separation within the layer either as a balanced or imbalanced dipole (or a multipole) of charge layers, while when the mean field is completely below the reference field, dust electrical activity characterization is inconclusive. This ground electric field reduction below the local fair weather field can be attributed to either the conductivity reduction due to dust acting as a passive neutral element, where the greater the conductivity reduction the lesser the electric field reduction, or to charge separation between areas of accumulated charge.

The electrified dust scheme is approximated either via the absence of dust charge separation or with thin cylindrical finite charge geometries (as opposed to infinite plate analogues) that allow explaining the electric field dependence on the layer height and the separation distance between the regions of charge accumulation. Both concepts have been suggested to explain the observed E-field responses at ground. However, there is no observational evidence up to now to validate the charge strata morphology, which might be far from similar to the elevated layers morphology due to the charged dust particles complex transport dynamics. To constrain the modelling formalism proposed here, future research will include profiling of the columnar electrical properties of dust, deploying airborne platforms (balloons and UAVs) within the Saharan Air Layer during foreseen future experiments at Cyprus and Cape Verde within ~~the years 2020 and~~ 2021.

Appendix A

~~3.3.1~~ Dust layer acting as a passive element

In Fig. A1~~Fig. 8.~~, the dependence of the near ground electric field strength, $E_{z_0,layer}$ (red line) of an electrically neutral dust layer on the conductivity reduction factor, the scale height, the layer central height and the layer depth, as given in (11), is plotted and compared to the fair weather electric field E_{z_0} at ground (blue line) which is given by (7). E_{z_0} depends only on the scale height and decreases as l increases, while it remains constant for the other varying parameters as expected from equation

Formatted: Indent: Left: 0", Hanging: 0.13", Outline numbered + Level: 1 + Numbering Style: 1, 2, 3, … + Start at: 1 + Alignment: Left + Aligned at: 0.25" + Indent at: 0.5"

Formatted: Font: Bold, No underline

Formatted: Heading 2

(7). The calculated fair weather field value of ~ 42 V/m, for the selected l, is comparable to the estimated value by Williams (2003) from Ohm's law, when dividing the globally integrated conduction current density by the mean atmospheric electrical conductivity at ground ($J_{z_0} \approx 2x10^{-12} A/m^2, \sigma_0 \approx 5x10^{-14} S/m$) and assuming an exponentially increasing conductivity profile above the Earth's surface (Haldoupis et al., 2017). We note that this globally averaged value of E_{z_0} is much less from the typically measured which is around 100 V/m (e.g., Corney et al., 2003; Reddell et al., 2004). We believe that the average value is more suitable for global calculations, because it incorporates the variations of the conductivity distribution around the Earth. On the other hand, the typical value is tied to the location of the measurement, and it varies at different locations as the conductivity distribution changes.

Consequently, $E_{z_0,layer}$ strongly depends on the conductivity reduction as depicted in the Fig. A1 case (a) curve, where the field reduces with the increasing reduction factor more effectively than with respect to the other three parameters, meaning that atmospheric conductivity reduction is the predominant factor that affects the E-field strength by largely lowering it. The E_{z_0} depends only on the varying scaling height as expected from equation (7).~~Consequently, $E_{z_0,layer}$ exhibits the greatest variation with the reduction factor n, meaning that atmospheric conductivity reduction is the predominant factor that affects the E-field strength by largely lowering it.~~

Authors Contribution: VD supervised the installation of the FM in both stations, collected and processed the data, constructed the reference field, provided physical input to the model and to the measurements' interpretation, plotted the lidar data and prepared the paper with contributions from all co-authors. SM conceptualized the model formalism and the processing chain of the reference field, also provided the key physical interpretation of the measurements. VA directed the preparation of the paper, supervised the study, offered his specialty in lidar data interpretation and gave insight to the E-field measurements. JU kindly conferred the FM, co-supervised the study and provided scientific consultation on both model outputs and E-field measurements. GH installed the FM on both stations, ensured the continuous data retrieval and gave insight to the E-field measurements. AG operated the lidar and supervised the data retrieval, provided the processed lidar data, along with dust layer base plots and aided on their interpretation. IT provided the VLDR data and helped on the selection of the dust cases according to these. Lastly, KT provided valuable scientific consultation concerning the E-field data, model assumptions and correlation to the dust layer proximity to the ground.

Acknowledgments: This research was supported by data and services obtained from the PANhellenic GEophysical Observatory of Antikythera (PANGEA) of NOA. The authors would like to acknowledge support of this work by the project "PANhellenic infrastructure for Atmospheric Composition and climatE change" (MIS 5021516) which is implemented under the Action "Reinforcement of the Research and Innovation Infrastructure", funded by the Operational Programme "Competitiveness, Entrepreneurship and Innovation" (NSRF 2014-2020) and co-financed by Greece and the European Union (European Regional Development Fund). We are grateful to EARLINET (https://www.earlinet.org/) and ACTRIS (https://www.actris.eu) for the data collection, calibration, processing and dissemination. VD would like to thank Dr. Eleni

Marinou for distributing the processing algorithm for the attenuated backscatter lidar retrievals. VD would also like to thank Prof. Charmandaris for his insightful comments and Dr. Nikos Kalivitis for his help in the data retrieval from Finokalia.

Financial Support: This research was supported by D-TECT (Grant Agreement 725698) funded by the European Research Council (ERC) under the European Union's Horizon 2020 research and innovation programme. VD would like to acknowledge that this research is also co-financed by Greece and the European Union (European Social Fund- ESF) through the Operational Programme «Human Resources Development, Education and Lifelong Learning» in the context of the project "Strengthening Human Resources Research Potential via Doctorate Research" (MIS-5000432), implemented by the State Scholarships Foundation (IKY)» and supported by the A. G. Leventis Foundation scholarship. Support was provided also from the Stavros Niarchos Foundation (SNF) in the form of a student scholarship. KT acknowledges funding from the European Research Council (ERC) under the European Unions Horizon 2020 research and innovation programme under grant agreement No. 771282.

Conflicts of Interest: The authors declare no conflict of interest.

References

Anisimov, S. V., Afinogenov, K. V. and Shikhova, N. M.: Dynamics of undisturbedmidlatitude atmospheric electricity: From observations to scaling, Radiophys. Quantum Electron., 56(11–12), 709–722, doi:10.1007/s11141-014-9475-z, 2014.

Anisimov, S. V., Galichenko, S. V. and Mareev, E. A.: Electrodynamic properties and height of atmospheric convective boundary layer, Atmos. Res., 194, 119–129, doi:10.1016/j.atmosres.2017.04.012, 2017.

Bailey, J., Ulanowski, Z., Lucas, P. W., Hough, J. H., Hirst, E. and Tamura, M.: The effect of airborne dust on astronomical polarization measurements, Mon. Not. R. Astron. Soc., 386(2), 1016–1022, doi:10.1111/j.1365-2966.2008.13088.x, 2008.

Baumgaertner, A. J. G., Lucas, G. M., Thayer, J. P. and Mallios, S. A.: On the role of clouds in the fair weather part of the global electric circuit, Atmos. Chem. Phys., 14(16), 8599–8610, doi:10.5194/acp-14-8599-2014, 2014.

Bering, E. A., Few, A. A. and Benbrook, J. R.: The global electric circuit, Phys. Today, 51(10), 24–30, doi:10.1063/1.882422, 1998.

Chalmers, J.A., 1967. Atmospheric Electricity, second ed. Pergamon press, Oxford, UK.

Chubb, J.: The measurement of atmospheric electric fields using pole mounted electrostatic fieldmeters, J. Electrostat., 72(4), 295–300, doi:10.1016/j.elstat.2014.05.002, 2014.

Chubb, J.: Comparison of atmospheric electric field measurements by a pole mounted fieldmeter and by a horizontal wire antenna, J. Electrostat., 73, 1–5, doi:10.1016/j.elstat.2014.10.003, 2015.

Corney, R. C., Burns, G. B., Michael, K., Frank-Kamenetsky, A. V., Troshichev, O. A., Bering, E. A., Papitashvili, V. O., Breed, A. M. and Duldig, M. L.: The influence of polar-cap convection on the geoelectric field at Vostok, Antarctica, J. Atmos. Solar-Terrestrial Phys., 65(3), 345–354, doi:10.1016/S1364-6826(02)00225-0, 2003.

van der Does, M., Knippertz, P., Zschenderlein, P., Giles Harrison, R. and Stuut, J. B. W.: The mysterious long-range transport of giant mineral dust particles, Sci. Adv., 4(12), 1–9, doi:10.1126/sciadv.aau2768, 2018.

Duff, N. and Lacks, D. J.: Particle dynamics simulations of triboelectric charging in granular insulator systems, J. Electrostat., 66(1–2), 51–57, doi:10.1016/j.elstat.2007.08.005, 2008.

Engelmann, R., Kanitz, T., Baars, H., Heese, B., Althausen, D., Skupin, A., Wandinger, U., Komppula, M., Stachlewska, I. S., Amiridis, V., Marinou, E., Mattis, I., Linné, H. and Ansmann, A.: The automated multiwavelength Raman polarization and water-vapor lidar PollyXT: The neXT generation, Atmos. Meas. Tech., 9(4), 1767–1784, doi:10.5194/amt-9-1767-2016, 2016.

Esposito, F., Molinaro, R., Popa, C. I., Molfese, C., Cozzolino, F., Marty, L., Taj-Eddine, K., Di Achille, G., Franzese, G., Silvestro, S. and Ori, G. G.: The role of the atmospheric electric field in the dust-lifting process, Geophys. Res. Lett., 43(10), 5501–5508, doi:10.1002/2016GL068463, 2016.

Ette, A. I. I.: The effect of the Harmattan dust on atmospheric electric parameters, J. Atmos. Terr. Phys., 33(2), 295–300, doi:10.1016/0021-9169(71)90208-X, 1971.

Flamant, C., Pelon, J., Flamant, P. H. and Durand, P.: Lidar determination of the entrainment zone thickness at the top of the unstable marine atmospheric boundary layer, Boundary-Layer Meteorol., 83(2), 247–284, doi:10.1023/A:1000258318944, 1997.

Forward, K. M., Lacks, D. J. and Mohan Sankaran, R.: Particle-size dependent bipolar charging of Martian regolith simulant, Geophys. Res. Lett., 36(13), 1–5, doi:10.1029/2009GL038589, 2009.

Freier G. D.: The Electric Field of a Large Dust Devil, October, (10), 1960–1960, 1960.

Freudenthaler, V., Esselborn, M., Wiegner, M., Heese, B., Tesche, M., Ansmann, A., Müller, D., Althausen, D., Wirth, M., Fix, A., Ehret, G., Knippertz, P., Toledano, C., Gasteiger, J., Garhammer, M. and Seefeldner, M.: Depolarization ratio profiling at several wavelengths in pure Saharan dust during SAMUM 2006, Tellus, Ser. B Chem. Phys. Meteorol., 61(1), 165–179, doi:10.1111/j.1600-0889.2008.00396.x, 2009.

Griffiths, D. J.: Instructor's Solution Manual for Introduction to Electrodynamics, 4th Edition, Reed College, Pearson, 2013.

Gringel W. and Mulheisen R.: Sahara dust concentration in the troposphere over the north Atlantic derived from measurements of air conductivity Beitr. Phys. Atmos. 51 121–8, 1978.

Gringel, W., J. M. Rosen, and D. J. Hoffmann.: Electrical structure from 0 to 30 km, in The Earth Electrical Environment, edited by E. P. Krider and R. G. Robie, pp. 166-182, Nat. Acad. Press, Washington, D.C., 1986.

Gunn, R.: Diffusion Charging of Atmospheric Droplets By Ions, and the Resulting Combination Coefficients, J. Meteorol., 11(5), 339–347, doi:10.1175/1520-0469(1954)011<0339:dcoadb>2.0.co;2, 1954.

Haarig, M., Ansmann, A., Althausen, D., Klepel, A., Groß, S., Freudenthaler, V., Toledano, C., Mamouri, R. E., Farrell, D. A., Prescod, D. A., Marinou, E., Burton, S. P., Gasteiger, J., Engelmann, R. and Baars, H.: Triple-wavelength depolarization-ratio profiling of Saharan dust over Barbados during SALTRACE in 2013 and 2014, Atmos. Chem. Phys., 17(17), 10767–10794, doi:10.5194/acp-17-10767-2017, 2017.

Haldoupis, C., Rycroft, M., Williams, E. and Price, C.: Is the “Earth-ionosphere capacitor” a valid component in the atmospheric global electric circuit?, J. Atmos. Solar-Terrestrial Phys., 164(August), 127–131, doi:10.1016/j.jastp.2017.08.012, 2017.

Harrison, R. G.: Ion-aerosol-cloud processes in the lower atmosphere, Rev. Geophys., 41(3), 1012, doi:10.1029/2002RG000114, 2003.

Harrison, R. G.: The Carnegie Curve, , (July 2012), 209–232, doi:10.1007/s10712-012-9210-2, 2013.

Harrison, R. G. and Ingram, W. J.: Air-earth current measurements at Kew, London, 1909-1979, Atmos. Res., 76(1–4), 49–64, doi:10.1016/j.atmosres.2004.11.022, 2005.

Harrison, R. G. and Nicoll, K. A.: Fair weather criteria for atmospheric electricity measurements, J. Atmos. Solar-Terrestrial Phys., 179(February), 239–250, doi:10.1016/j.jastp.2018.07.008, 2018.

Harrison, R. G., Nicoll, K. A., Ulanowski, Z. and Mather, T. A.: Self-charging of the Eyjafjallajökull volcanic ash plume, Environ. Res. Lett., 5(2), 3–7, doi:10.1088/1748-9326/5/2/024004, 2010.

Harrison, R. G., Barth, E., Esposito, F., Merrison, J., Montmessin, F., Aplin, K. L., Borlina, C., Berthelier, J. J., Déprez, G., Farrell, W. M., Houghton, I. M. P., Renno, N. O., Nicoll, K. A., Tripathi, S. N. and Zimmerman, M.: Applications of Electrified Dust and Dust Devil Electrodynamics to Martian Atmospheric Electricity, Space Sci. Rev., 203(1–4), 299–345, doi:10.1007/s11214-016-0241-8, 2016.

Harrison, R. G., Nicoll, K. A., Marlton, G. J., Ryder, C. L. and Bennett, A. J.: Saharan dust plume charging observed over the UK, Environ. Res. Lett., 13(5), doi:10.1088/1748-9326/aabcd9, 2018.

Ilin, N. V., Slyunyaev, N. N. and Mareev, E. A.: Toward a Realistic Representation of Global Electric Circuit Generators in Models of Atmospheric Dynamics, J. Geophys. Res. Atmos., 125(6), 1–24, doi:10.1029/2019JD032130, 2020.

Inculet, I. I., Castle, G. S. P. and Aartsen, G.: Generation of bipolar electric fields during industrial handling of powders, Chem. Eng. Sci., 61(7), 2249–2253, doi:10.1016/j.ces.2005.05.005, 2006.

Kalinin, A. V., Slyunyaev, N. N., Mareev, E. A. and Zhidkov, A. A.: Stationary and nonstationary models of the global electric circuit: Well-posedness, analytical relations, and numerical implementation, Izv. - Atmos. Ocean Phys., 50(3), 314–322, doi:10.1134/S0001433814030074, 2014.

Kamra, a. K.: Measurements of the electrical properties of dust storms, J. Geophys. Res., 77(30), 5856, doi:10.1029/JC077i030p05856, 1972.

Kanagy, S. P. and Mann, C. J.: Electrical properties of eolian sand and silt, Earth Sci. Rev., 36(3–4), 181–204, doi:10.1016/0012-8252(94)90057-4, 1994.

Katz, S., Yair, Y., Price, C., Yaniv, R., Silber, I., Lynn, B. and Ziv, B.: Electrical properties of the 8–12th September, 2015 massive dust outbreak over the Levant, Atmos. Res., 201(November 2017), 218–225, doi:10.1016/j.atmosres.2017.11.004, 2018.

Kok, J. F. and Renno, N. O.: Enhancement of the emission of mineral dust aerosols by electric forces, Geophys. Res. Lett., 33(19), 2–6, doi:10.1029/2006gl026284, 2006.

Kourtidis, K., Szabóné André, K., Karagioras, A., Nita, I. A., Sátori, G., Bór, J. and Kastelis, N.: The influence of circulation weather types on the exposure of the biosphere to atmospheric electric fields, Int. J. Biometeorol., doi:10.1007/s00484-020-01923-y, 2020.

Krehbiel, P. R., Riousset, J. A., Pasko, V. P., Thomas, R. J., Rison, W., Stanley, M. A. and Edens, H. E.: Upward electrical discharges from thunderstorms, Nat. Geosci., 1(4), 233–237, doi:10.1038/ngeo162, 2008.

Lacks, D. J. and Shinbrot, T.: Long-standing and unresolved issues in triboelectric charging, Nat. Rev. Chem., 3(8), 465–476, doi:10.1038/s41570-019-0115-1, 2019.

Lelieveld, J., Berresheim, H., Borrmann, S., Crutzen, P. J., Dentener, F. J., Fischer, H., Feichter, J., Flatau, P. J., Heland, J., Holzinger, R., Korrmann, R., Lawrence, M. G., Levin, Z., Markowicz, K. M., Mihalopoulos, N., Minikin, A., Ramanathan, V., De Reus, M., Roelofs, G. J., Scheeren, H. A., Sciare, J., Schlager, H., Schultz, M., Siegmund, P., Steil, B., Stephanou, E. G., Stier, P., Traub, M., Warneke, C., Williams, J. and Ziereis, H.: Global air pollution crossroads over the Mediterranean, Science (80-.)., 298(5594), 794–799, doi:10.1126/science.1075457, 2002.

Long, Z. and Yao, Q.: Evaluation of various particle charging models for simulating particle dynamics in electrostatic precipitators, J. Aerosol Sci., 41(7), 702–718, doi:10.1016/j.jaerosci.2010.04.005, 2010.

Mallios, S. A. and Pasko, V. P.: Charge transfer to the ionosphere and to the ground during thunderstorms, J. Geophys. Res. Sp. Phys., 117(8), 1–16, doi:10.1029/2011JA017061, 2012.

Mallios, S. A., Daskalopoulou, V. and Amiridis, V.: Orientation of non spherical prolate dust particles moving vertically in the Earth's atmosphere, J. Aerosol Sci., 151(August 2020), 105657, doi:10.1016/j.jaerosci.2020.105657, 2021.

Mattis, I., Müller, D., Ansmann, A., Wandinger, U., Preißler, J., Seifert, P. and Tesche, M.: Ten years of multiwavelength Raman lidar observations of free-tropospheric aerosol layers over central Europe: Geometrical properties and annual cycle, J. Geophys. Res. Atmos., 113(20), 1–19, doi:10.1029/2007JD009636, 2008.

Nicoll, K., Harrison, G., Marlton, G. and Airey, M.: Consistent dust electrification from Arabian Gulf sea breezes, Environ. Res. Lett., 15(8), doi:10.1088/1748-9326/ab9e20, 2020.

Nicoll, K. A., Harrison, R. G. and Ulanowski, Z.: Observations of Saharan dust layer electrification, Environ. Res. Lett., 6(1), 1–8, doi:10.1088/1748-9326/6/1/014001, 2011.

Reddell, B. D., Benbrook, J. R., Bering, E. A., Cleary, E. N. and Few, A. A.: Seasonal variations of atmospheric electricity measured at Amundsen-Scott South Pole Station, J. Geophys. Res. Sp. Phys., 109(A9), 1–17, doi:10.1029/2004JA010536, 2004.

Renno, N. O. and Kok, J. F.: Electrical activity and dust lifting on earth, Mars, and beyond, Space Sci. Rev., 137(1–4), 419–434, doi:10.1007/s11214-008-9377-5, 2008.

Riousset, J. A., Pasko, V. P., Krehbiel, P. R., Thomas, R. J. and Rison, W.: Three-dimensional fractal modeling of intracloud lightning discharge in a New Mexico thunderstorm and comparison with lightning mapping observations, J. Geophys. Res. Atmos., 112(15), 1–17, doi:10.1029/2006JD007621, 2007.

Rycroft, M. J., Harrison, R. G., Nicoll, K. A. and Mareev, E. A.: An overview of earth's global electric circuit and atmospheric conductivity, Space Sci. Rev., 137(1–4), 83–105, doi:10.1007/s11214-008-9368-6, 2008.

Ryder, C. L., Marenco, F., Brooke, J. K., Estelles, V., Cotton, R., Formenti, P., McQuaid, J. B., Price, H. C., Liu, D., Ausset, P., Rosenberg, P., Taylor, J. W., Choularton, T., Bower, K., Coe, H., Gallagher, M., Crosier, J., Lloyd, G., Highwood, E. J. and Murray, B. J.: Coarse mode mineral dust size distributions, composition and optical properties from AER-D aircraft measurements over the Tropical Eastern Atlantic, Atmos. Chem. Phys. Discuss., 98, 1–49, doi:10.5194/acp-2018-739, 2018.

Siingh, D., Gopalakrishnan, V., Singh, R. P., Kamra, A. K., Singh, S., Pant, V., Singh, R. and Singh, A. K.: The atmospheric global electric circuit: An overview, Atmos. Res., 84(2), 91–110, doi:10.1016/j.atmosres.2006.05.005, 2007.

Silva, H. G., Lopes, F. M., Pereira, S., Nicoll, K., Barbosa, S. M., Conceição, R., Neves, S., Harrison, R. G. and Collares Pereira, M.: Saharan dust electrification perceived by a triangle of atmospheric electricity stations in Southern Portugal, J. Electrostat., 84, 106–120, doi:10.1016/j.elstat.2016.10.002, 2016.

Solomos, S., Kalivitis, N., Mihalopoulos, N., Amiridis, V., Kouvarakis, G., Gkikas, A., Binietoglou, I., Tsekeri, A., Kazadzis, S., Kottas, M., Pradhan, Y., Proestakis, E., Nastos, P. T. and Marenco, F.: From tropospheric folding to Khamsin and Foehn winds: How atmospheric dynamics advanced a record-breaking dust episode in Crete, Atmosphere (Basel)., 9(7), doi:10.3390/atmos9070240, 2018.

Stolzenburg, M. and Marshall, T. C.: Charge structure and dynamics in thunderstorms, Space Sci. Rev., 137(1–4), 355–372, doi:10.1007/s11214-008-9338-z, 2008.

Tegen, I., Hollrig, P., Chin, M., Fung, I., Jacob, D. and Penner, J.: Contribution of different aerosol species to the global aerosol extinction optical thickness: Estimates from model results, J. Geophys. Res. Atmos., 102(20), 23895–23915, doi:10.1029/97jd01864, 1997.

Tinsley, B. A. and Zhou, L.: Initial results of a global circuit model with variable stratospheric and tropospheric aerosols, , 111(August), 1–23, doi:10.1029/2005JD006988, 2006.

Ulanowski, Z., Bailey, J., Lucas, P., Hough, J. and Hirst, E.: Alighnment of atmospheric mineral dust due to electric field, Atmos. Chem. Phys., 7, 6161–6173, 2007.

Veselovskii, I., Goloub, P., Podvin, T., Bovchaliuk, V., Derimian, Y., Augustin, P., Fourmentin, M., Tanre, D., Korenskiy, M., Whiteman, D. N., Diallo, A., Ndiaye, T., Kolgotin, A. and Dubovik, O.: Retrieval of optical and physical properties of African dust from multiwavelength Raman lidar measurements during the SHADOW campaign in Senegal, Atmos. Chem. Phys., 16(11), 7013–7028, doi:10.5194/acp-16-7013-2016, 2016.

Veselovskii, I., Hu, Q., Goloub, P., Podvin, T., Korenskiy, M., Derimian, Y., Legrand, M. and Castellanos, P.: Variability in lidar-derived particle properties over West Africa due to changes in absorption: Towards an understanding, Atmos. Chem. Phys., 20(11), 6563–6581, doi:10.5194/acp-20-6563-2020, 2020.

Waitukaitis, S. R., Lee, V., Pierson, J. M., Forman, S. L. and Jaeger, H. M.: Size-dependent same-material tribocharging in insulating grains, Phys. Rev. Lett., 112(21), 1–5, doi:10.1103/PhysRevLett.112.218001, 2014.

Whitby K. T., Liu B. Y. H.: The electrical behaviour of aerosols, Aerosol Science, C. N. Davies, Ed., Academic Press, 1966.

Williams, E. R.: The global electrical circuit: A review, Atmos. Res., 91(2–4), 140–152, doi:10.1016/j.atmosres.2008.05.018, 2009.

Wright, H. L.: The influence of atmospheric suspensoids upon the earth's electric field as indicated by observations at kew observatory, Proc. Phys. Soc., 45(2), 152–171, doi:10.1088/0959-5309/45/2/303, 1933.

Yair, Y., Katz, S., Yaniv, R., Ziv, B. and Price, C.: An electrified dust storm over the Negev desert, Israel, Atmos. Res., 181, 63–71, doi:10.1016/j.atmosres.2016.06.011, 2016.

Yaniv, R., Yair, Y., Price, C. and Katz, S.: Local and global impacts on the fair-weather electric field in Israel, Atmos. Res., 172–173, 119–125, doi:10.1016/j.atmosres.2015.12.025, 2016.

Yaniv, R., Yair, Y., Price, C., Mkrtchyan, H., Lynn, B. and Reymers, A.: Ground-based measurements of the vertical E-field in mountainous regions and the "Austausch" effect, Atmos. Res., 189, 127–133, doi:10.1016/j.atmosres.2017.01.018, 2017.

Zhang, H. and Zhou, Y. H.: Reconstructing the electrical structure of dust storms from locally observed electric field data, Nat. Commun., 11(1), doi:10.1038/s41467-020-18759-0, 2020.

Zheng, X.-J.: Electrification of wind-blown sand: Recent advances and key issues, Eur. Phys. J. E, 36(12), 138, doi:10.1140/epje/i2013-13138-4, 2013.

Zhou, L. and Tinsley, B. A.: Production of space charge at the boundaries of layer clouds, J. Geophys. Res. Atmos., 112(11), 1–17, doi:10.1029/2006JD007998, 2007.

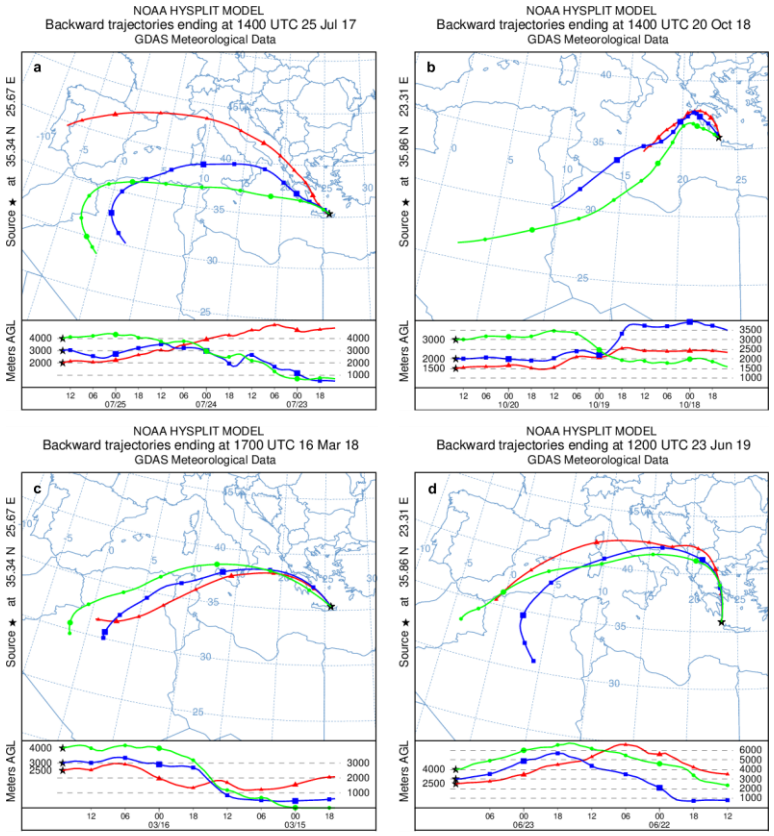

Fig. 1. NOAA HYSPLIT back trajectories model with GDAS assimilated data input for: (a) 25/07/2017 –with 72 ~~hrs~~ hrs backward propagation of air masses ~~(~~towards Fin~~.),~~ okalia, (b) 20/10/2018 –with 72 hrs backward propagation of air masses towards ~~(~~Antik~~.)~~ythera, (c) 16/03/2018 –with 48 hrs backward propagation of air masses towards ~~(~~Fin~~.)~~ okalia and (d) 23/06/2019 –with 48 hrs backward propagation of air masses towards ~~(~~Antik~~.)~~ythera ~~backward propagation of air masses~~(https://www.ready.noaa.gov/HYSPLIT.php).

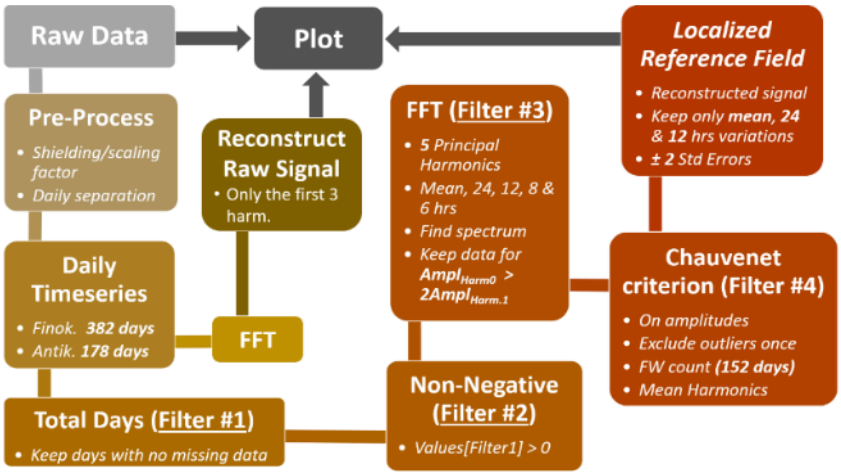

Fig. 2. Signal processing chain for: (i) the derivation of the Localized Reference Electric Field (LREF) that represents the local fair weather conditions, following the proposed filtering process (Filters no. 1 to no. 4, yellow-to-orange) of the field mill electric field data as retrieved on both Finokalia and Antikythera atmospheric stations and (ii) the derivation of the daily mean electric field under dust driven days from the same datasets (yellow-to-olive green). The LREF is compared to the mean electric field values in order to assess the electric field behaviour.

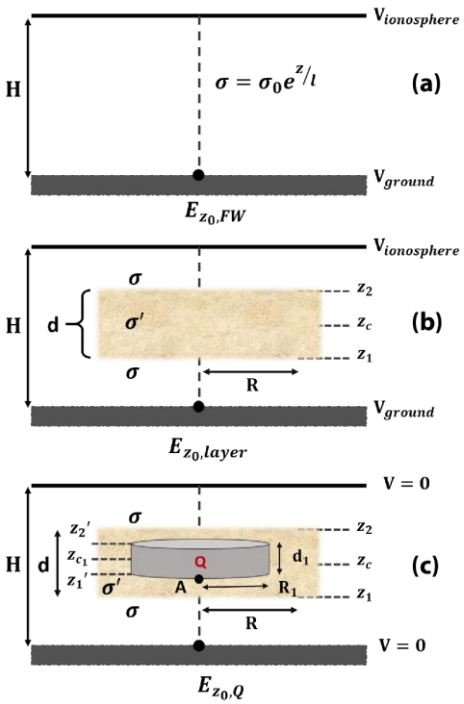

Fig. 3. Schematic of the formalism for the calculation of the steady state ~~surface~~ near-ground electric field bounded between the ground potential (V_{ground}) and ionospheric potential ($V_{ionosphere}$) at height H, under: (a) fair weather conditions ($E_{z_{0,FW}}$) where atmospheric conductivity σ, follows an exponential distribution along the altitude z with respect to the scaling height l, (b) the presence of an electrically neutral dust layer ($E_{z_{0,layer}}$) with depth d and radius R, which ~~reduces~~ modifies conductivity to σ' and (c) the hypothesis of a cylindrical charged monopole ($E_{z_{0,Q}}$) within the dust layer, with depth d_1, radius R_1 and total charge Q. The monopole case is a superposition of the electrically neutral dust layer with the charged cylinder within ~~a~~ the bounded atmospheric potential.

Table 1. Dust layer central height and depth, as derived from the ~~V~~PLDR ~~plots~~profiles.

Dust Outbreak	z_{c_i} (km)	d_i (km)
25/07/2017 (Fin.)	3	4
20/10/2018 (Ant.)	3	4
16/03/2018 (Fin.)	3.5	2.5
23/06/2019 (Ant.)	3.5	3

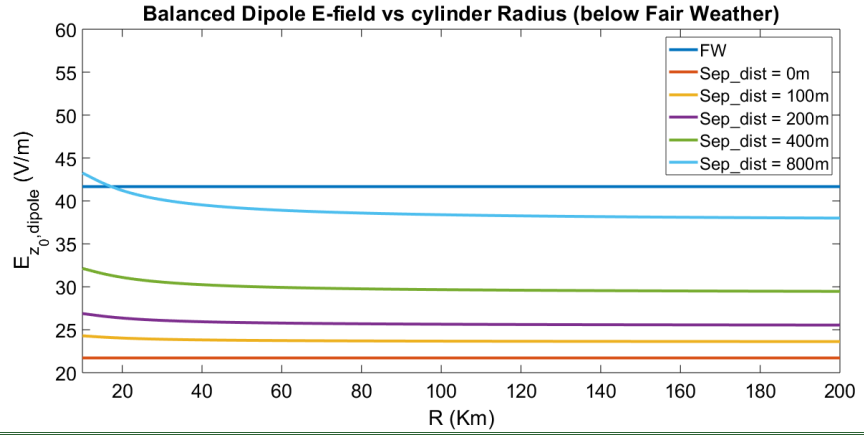

Fig. 9. Vertical electric field strength at ground level for a dipole of finite uniformly charged cylinders $E_{z_0,dipole}$, within an elevated dust layer as a function of the cylinder radius R. $E_{z_0,dipole}$ is calculated for relatively small separation distances between the charged layers. As the separation distance increases, the E-field increases due to the stronger influence of the lower cylinder to the surface resistance as it moves towards the ground, but the enhancement is not significant enough to overcome the fair weather values.

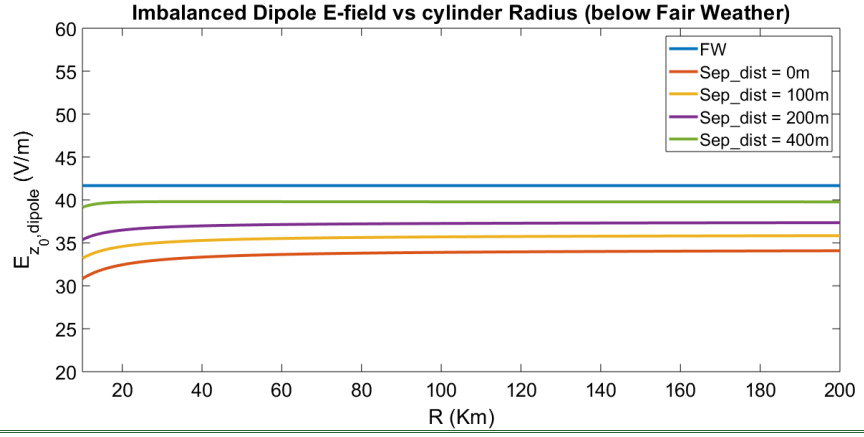

Fig. 10. Vertical electric field strength at ground level for an imbalanced dipole of finite charged cylinders $E_{z_0,dipole}$, within an elevated dust layer as a function of the cylinder radius R. $E_{z_0,dipole}$ is calculated for relatively small separation distances. Dipole exhibits charge imbalance of 8% (relative charge density difference), with the upper negative cylinder having smaller charge density. As the charged layers move apart the E-field increases more rapidly than in the case of balanced charges, for the same separation distances, since the influence of the upper cylinder is dominant. The effect is, again, not significant enough to overcome the fair weather values but the dust layer is stratified.

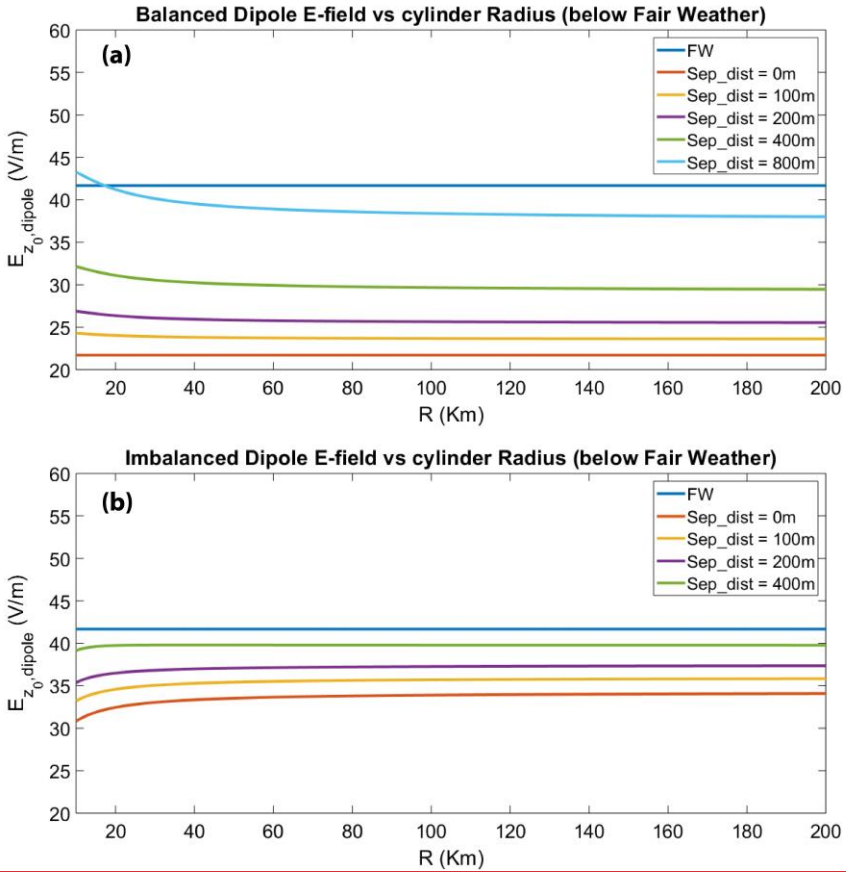

Fig. 4. Vertical electric field strength at ground level ($E_{z_{0,dipole}}$) below the fair weather field (blue line), for a dipole of: (a) finite uniformly charged cylinders and (b) non uniformly charged cylinders exhibiting a charge imbalance of 8%, within an elevated dust layer as a function of the cylinder radius *R*. $E_{z_{0,dipole}}$ is calculated for separation distances of 0 (electrically neutral dust), 100, 200, 400 and 800 m (balanced dipole case only) between the charged layers.

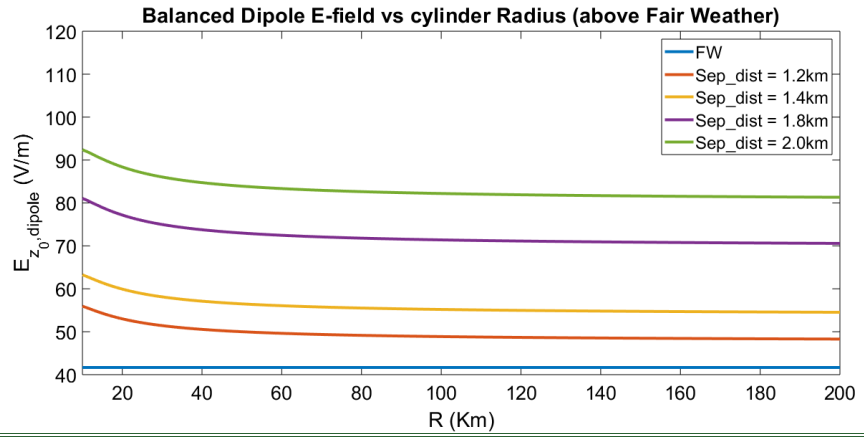

~~Fig. 11. Vertical electric field strength at ground level for a dipole of finite uniformly charged cylinders $E_{z_0,dipole}$ within an elevated dust layer as a function of the cylinder radius R. The E-field is calculated for separation distances over 1 km between the two charged layers, which results in significant enhancement of the electric field above the fair weather values. The influence of the lower cylinder to the ground E-field becomes more prominent as the separation distance increases.~~

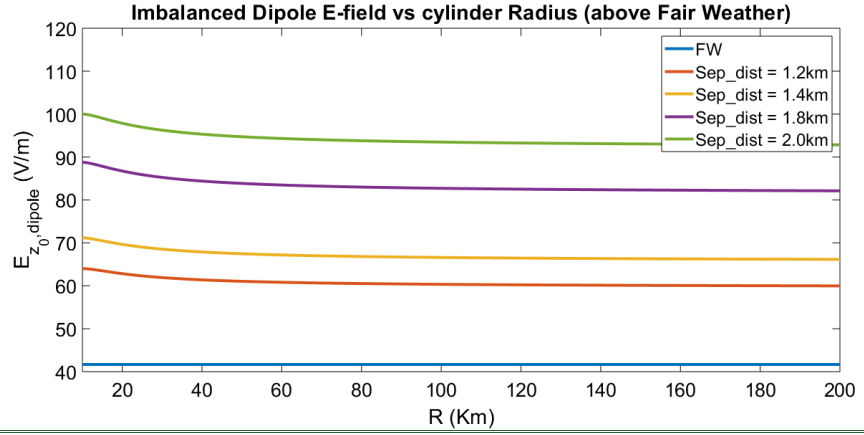

~~Fig. 12. Vertical electric field strength at ground level for an imbalanced dipole of finite charged cylinders $E_{z_0,dipole}$ within an elevated dust layer as a function of the cylinder radius R. The E-field is calculated for separation distances over 1 km between the two charged layers, which results in significant enhancement of the electric field above the fair weather values. The dipole exhibits a charge imbalance of 8%, with the upper negative cylinder having smaller charge density. For these separation distances, the effect to the electric field is significant enough to overcome the calculated fair weather values.~~

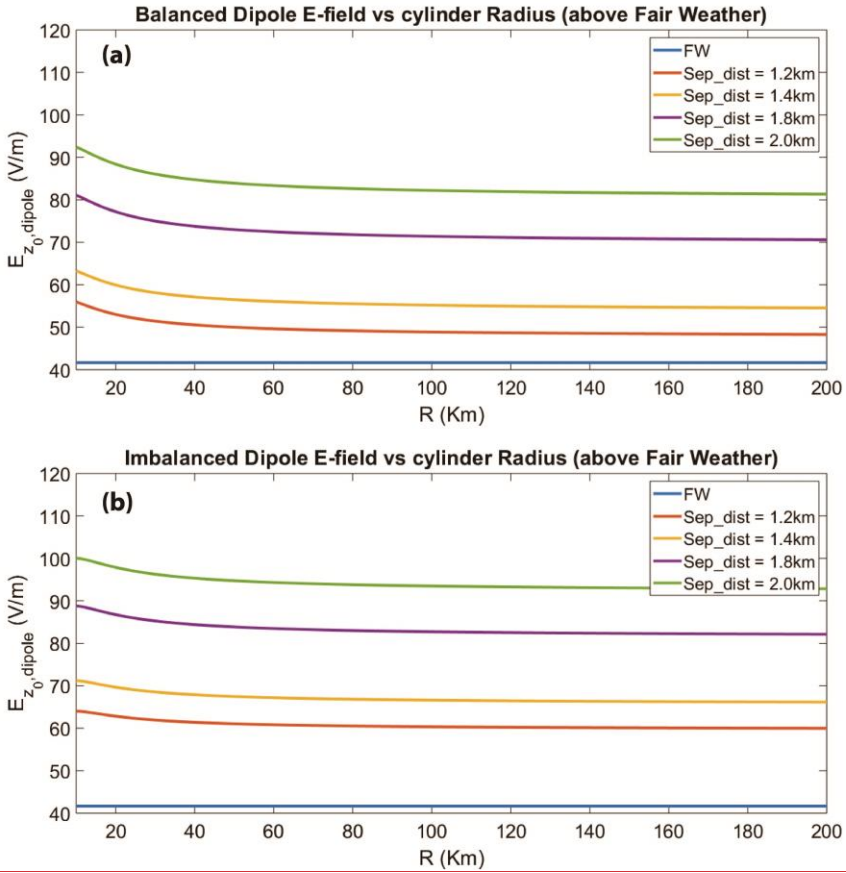

Fig. 5. Vertical electric field strength at ground level ($E_{z_{0,dipole}}$) above the fair weather field (blue line), for a dipole of: (a) finite uniformly charged cylinders and (b) non uniformly charged cylinders exhibiting a charge imbalance of 8%, within an elevated dust layer as a function of the cylinder radius *R*. $E_{z_{0,dipole}}$ is calculated for separation distances of 1.2, 1.4, 1.8 and 2 km between the two charged layers.

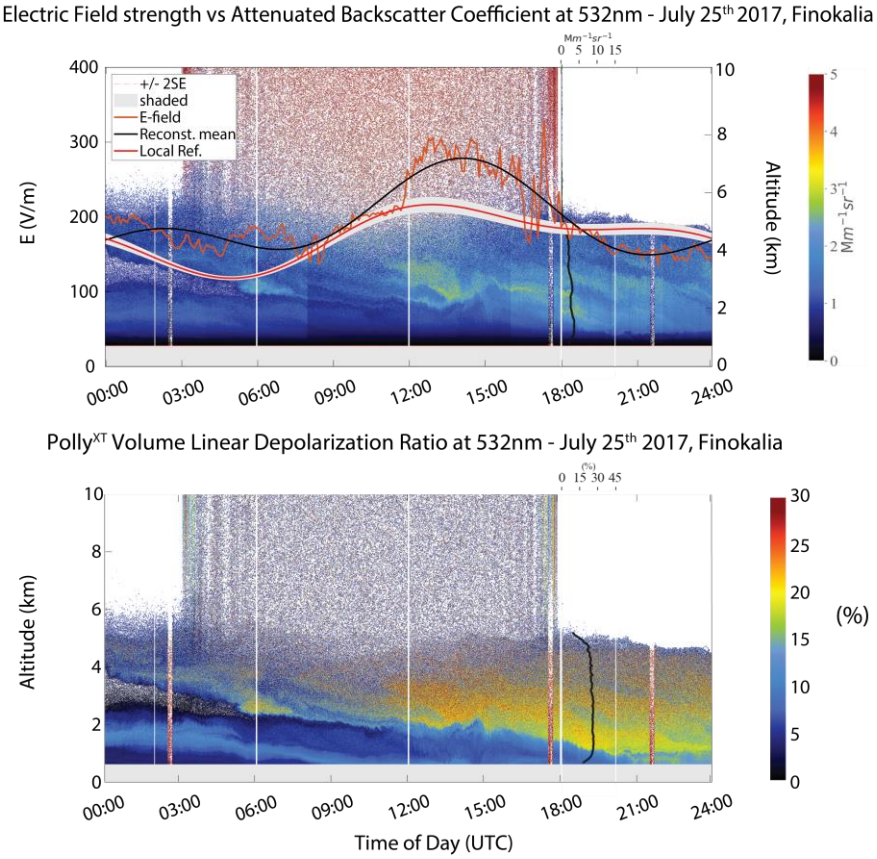

Fig. 6. Top panel: Timeseries of the vertical electric field strength (orange), the extracted Localized Reference Electric Field (red) and the reconstructed mean electric field variation (black) from the field mill dataset, for the recorded 25/07/2017 dust layer in Finokalia. The E-field data are plotted with the time-height evolution of the attenuated backscatter coefficient ($Mm^{-1}sr^{-1}$) and the particle backscatter coefficient (β) profile ($Mm^{-1}sr^{-1}$, black vertical line) at 532 nm from the Polly^{XT} lidar, which was co-located with the field mill. Areas of increased particle concentration are denoted with reddish tones, while the β values are derived by averaging between 18:00 and 21:00 (UTC). Bottom panel: Volume Linear Depolarization Ratio (δ_v, %) at 532 nm for the same dust layer as obtained from the Polly^{XT} lidar and the Particle Linear Depolarization Ratio (δ_p, %) profile (black vertical line) again averaged between 18:00 and 21:00 (UTC). Large δ_v values are depicted with reddish tones. ~~Timeseries of the vertical electric field strength (orange), the Localized Reference Electric Field (red) and the reconstructed mean electric field variation (black) plotted with the Total Attenuated backscatter coefficient against the altitude, for the 25/07/2017 dust layer in Finokalia. Areas of increased particle concentration are denoted with reddish tones. The mean E-field is consistently above the reference field.~~ Bottom panel: ~~Volume~~

~~Linear Depolarization Ratio (%) for the same dust layer as obtained from the Polly^{XT} lidar. VLDR values between 25% and 30% indicate the presence of mostly mixed dust within the layer.~~

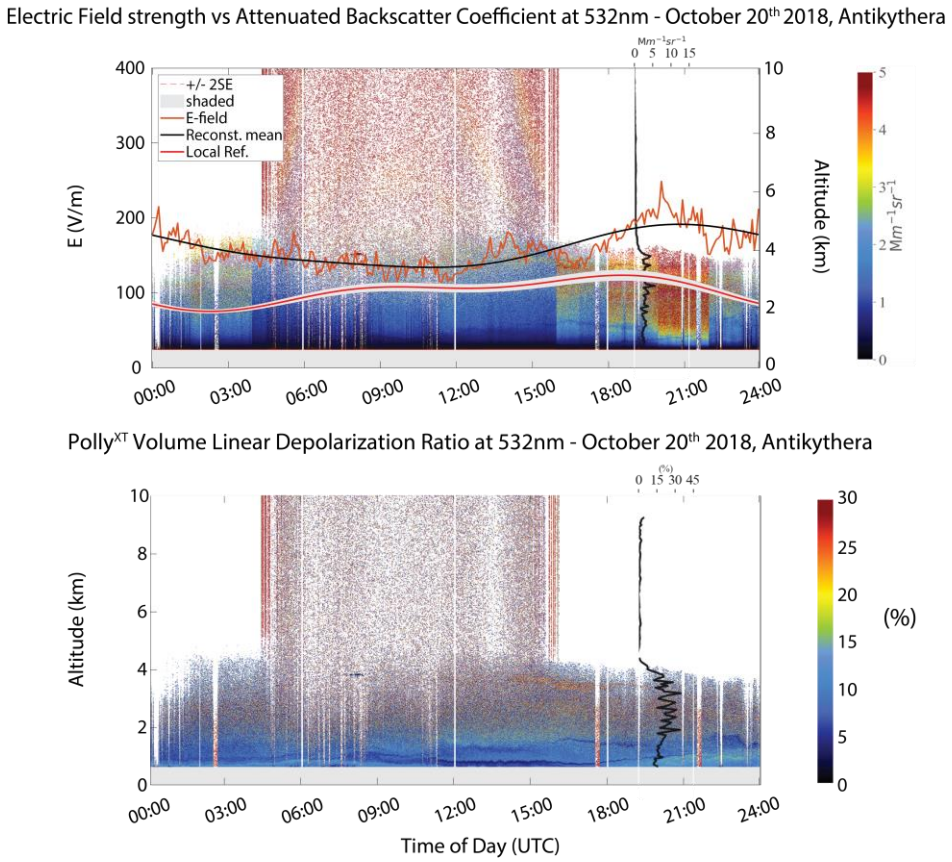

Fig. 7. **Top panel:** Timeseries of the vertical electric field strength (orange), the extracted Localized Reference Electric Field (red) and the reconstructed mean electric field variation (black) from the field mill dataset, for the recorded 20/10/2018 dust layer in Antikythera. The E-field data are plotted with the time-height evolution of the attenuated backscatter coefficient ($Mm^{-1}sr^{-1}$) and the particle backscatter coefficient (β) profile ($Mm^{-1}sr^{-1}$, black vertical line) at 532 nm from the Polly^{XT} lidar, which was co-located with the field mill. Areas of increased particle concentration are denoted with red tones, while the β values are derived by averaging between 18:00 and 21:00 (UTC). Bottom panel: Volume Linear Depolarization Ratio (δ_v, %) at 532 nm for the same dust layer as obtained from the Polly^{XT} lidar and the Particle Linear Depolarization Ratio (δ_p, %) profile (black vertical line) again averaged

between 18:00 and 21:00 (UTC). Large δ_v values are depicted with red tones. ~~Timeseries of the vertical electric field strength (orange), the Localized Reference Electric Field (red) and the reconstructed mean electric field variation (black), plotted with the Total Attenuated backscatter coefficient against the altitude, for the 20/10/2018 dust layer in Antikythera. Areas of increased particle concentration are denoted again with reddish tones. The mean E-field is consistently above the reference field, showing an increase at ~2100 UTC, when dust deposition becomes prominent. Bottom panel: Volume Linear Depolarization Ratio (%) for the same dust layer as obtained from the Polly^{XT} lidar. VLDR values between 25% and 30% indicate the presence of mostly mixed dust within the layer.~~

Formatted: Justified

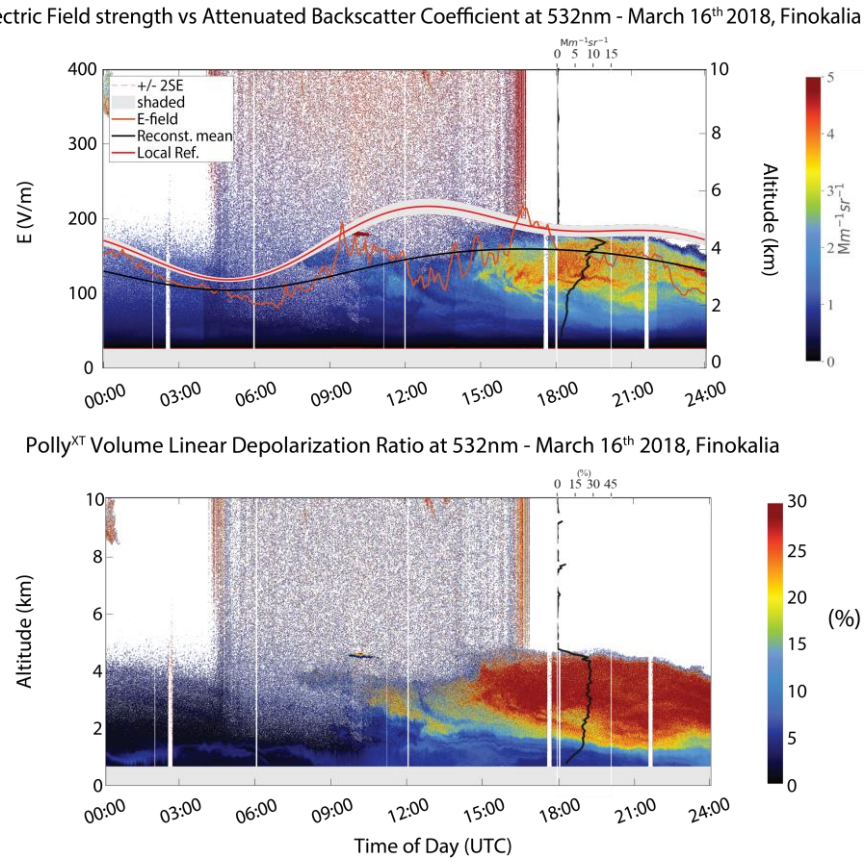

Fig. 8. Top panel: Timeseries of the vertical electric field strength (orange), the extracted Localized Reference Electric Field (red) and the reconstructed mean electric field variation (black) from the field mill dataset, for the recorded 16/03/2018 dust layer in

Finokalia. The E-field data are plotted with the time-height evolution of the attenuated backscatter coefficient ($Mm^{-1}sr^{-1}$) and the particle backscatter coefficient (β) profile ($Mm^{-1}sr^{-1}$, black vertical line) at 532 nm from the Polly^{XT} lidar, which was co-located with the field mill. Areas of increased particle concentration are denoted with red tones, while the β values are derived by averaging between 18:00 and 21:00 (UTC). Bottom panel: Volume Linear Depolarization Ratio (δ_v, %) at 532 nm for the same dust layer as obtained from the Polly^{XT} lidar and the Particle Linear Depolarization Ratio (δ_p, %) profile (black vertical line) again averaged between 18:00 and 21:00 (UTC). Large δ_v values are depicted with red tones. ~~Timeseries of the vertical electric field strength (orange), the Localized Reference Electric Field (red) and the reconstructed mean electric field variation (black), plotted with the Total Attenuated backscatter coefficient against the altitude, for the 16/03/2018 dust layer in Finokalia. Areas of increased particle concentration are denoted with red tones. The mean E-field remains positive and well below the reference field, exhibiting an increase as particle injection initiates at ~1100 UTC and then a decrease along the plume's progression. Bottom panel: Volume Linear Depolarization Ratio (%) for the same dust layer as obtained from the Polly^{XT} lidar. VLDR values between 35% and 40% indicate a pure dust layer within 1.5 km and 4 km, with no surface dust concentration.~~

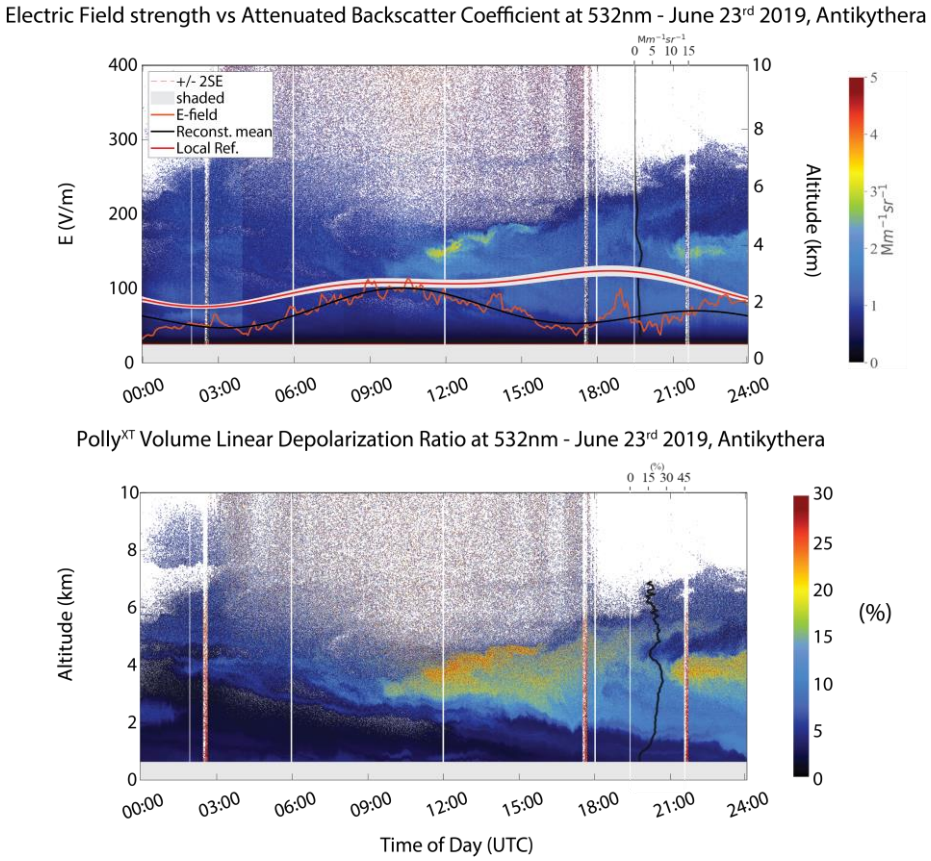

Fig. 9. Top panel: Timeseries of the vertical electric field strength (orange), the extracted Localized Reference Electric Field (red) and the reconstructed mean electric field variation (black) from the field mill dataset, for the recorded 23/06/2019 dust layer in Antikythera. The E-field data are plotted with the time-height evolution of the attenuated backscatter coefficient ($Mm^{-1}sr^{-1}$) and the particle backscatter coefficient (β) profile ($Mm^{-1}sr^{-1}$, black vertical line) at 532 nm from the Polly^{XT} lidar, which was co-located with the field mill. Areas of increased particle concentration are denoted with reddish tones, while the β values are derived by averaging between 18:00 and 21:00 (UTC). Bottom panel: Volume Linear Depolarization Ratio (δ_v, %) at 532 nm for the same dust layer as obtained from the Polly^{XT} lidar and the Particle Linear Depolarization Ratio (δ_p, %) profile (black vertical line) again averaged between 18:00 and 21:00 (UTC). Large δ_v values are depicted with reddish tones. ~~Timeseries of the vertical electric field strength (orange), the Localized Reference Electric Field (red) and the reconstructed mean electric field variation (black), plotted with the Total Attenuated backscatter coefficient against the altitude, for the 23/06/2019 dust layer in Antikythera. Areas of increased particle~~

concentration are denoted with red tones. The mean E field is positive and consistently below the reference field, exhibiting an increase when particle injection begins towards noon and further drops as the layer progresses to lower altitudes. Bottom panel: Volume Linear Depolarization Ratio (%) for the same dust layer as obtained from the Polly^{XT} lidar. VLDR values between 35% and 40% indicate a pure dust layer within 2 km and 4.5 km, with no surface dust concentration.

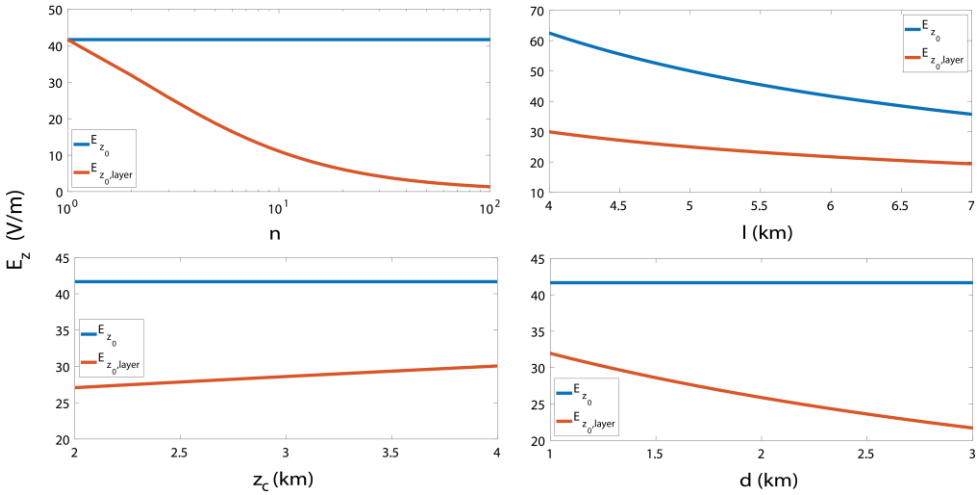

Fig. 8. Dependence of the vertical electric field, at ground level, under fair weather (E_{z_0}, blue line) and under the influence of an uncharged dust layer ($E_{z_0,layer}$, red line) on: (a) the reduction factor n, (b) the scaling height l, (c) the central layer height z_c and (d) the separation distance d, for $1/\sigma_0 = 3 \cdot 10^{12}$ Ω m, $V_{tot} = 250$ kV and H = 70 km. $E_{z_0,layer}$ strongly depends on the conductivity reduction as depicted in the case (a) curve, where the field reduces with the increasing reduction factor more effectively than with respect to the other three parameters. E_{z_0} depends only on the scaling height as expected.

Table 1. Dust layer central height and depth, as derived from the VLDR plots.

Dust Outbreak:	z_{c_i} (km)	d_i (km)
25/07/2017 (Fin.)	3	4
20/10/2018 (Ant.)	3	4
16/03/2018 (Fin.)	3.5	2.5
23/06/2019 (Ant.)	3.5	3

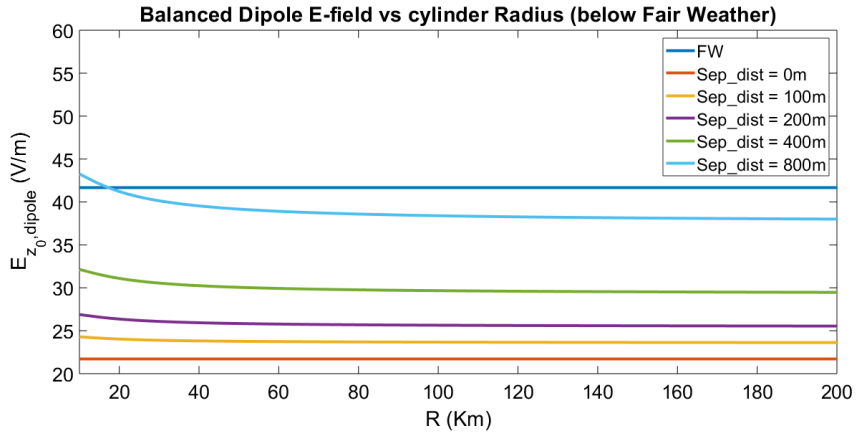

~~Fig. 9. Vertical electric field strength at ground level for a dipole of finite uniformly charged cylinders $E_{z_0,dipole}$, within an elevated dust layer as a function of the cylinder radius R. $E_{z_0,dipole}$ is calculated for relatively small separation distances between the charged layers. As the separation distance increases, the E-field increases due to the stronger influence of the lower cylinder to the surface resistance as it moves towards the ground, but the enhancement is not significant enough to overcome the fair-weather values.~~

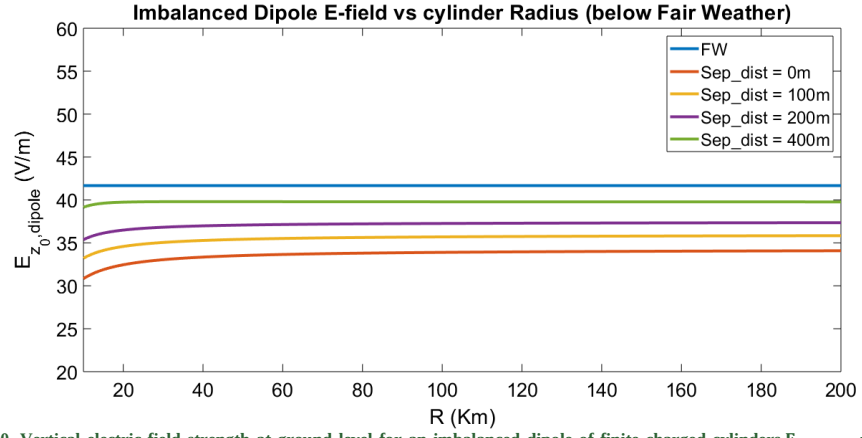

~~Fig. 10. Vertical electric field strength at ground level for an imbalanced dipole of finite charged cylinders $E_{z_0,dipole}$, within an elevated dust layer as a function of the cylinder radius R. $E_{z_0,dipole}$ is calculated for relatively small separation distances. Dipole exhibits charge imbalance of 8% (relative charge density difference), with the upper negative cylinder having smaller charge density. As the charged layers move apart the E-field increases more rapidly than in the case of balanced charges, for the same separation distances, since the influence of the upper cylinder is dominant. The effect is, again, not significant enough to overcome the fair weather values but the dust layer is stratified.~~

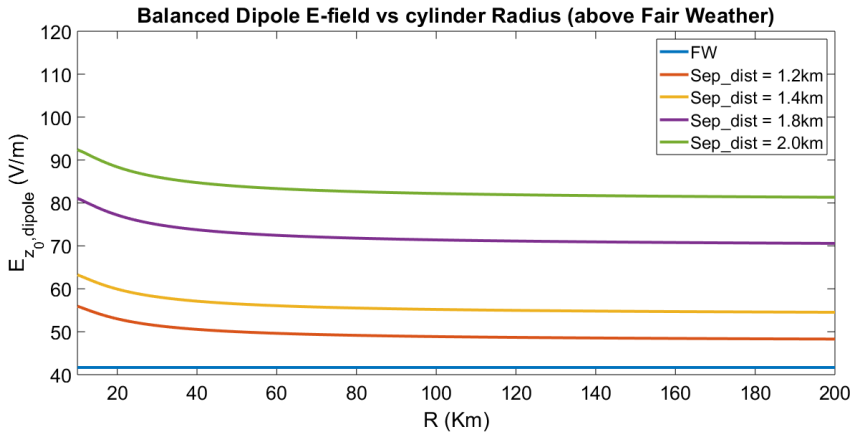

Fig. 11. Vertical electric field strength at ground level for a dipole of finite uniformly charged cylinders $E_{z_0,dipole}$, within an elevated dust layer as a function of the cylinder radius *R*. The E-field is calculated for separation distances over 1 km between the two charged layers, which results in significant enhancement of the electric field above the fair weather values. The influence of the lower cylinder to the ground E-field becomes more prominent as the separation distance increases.

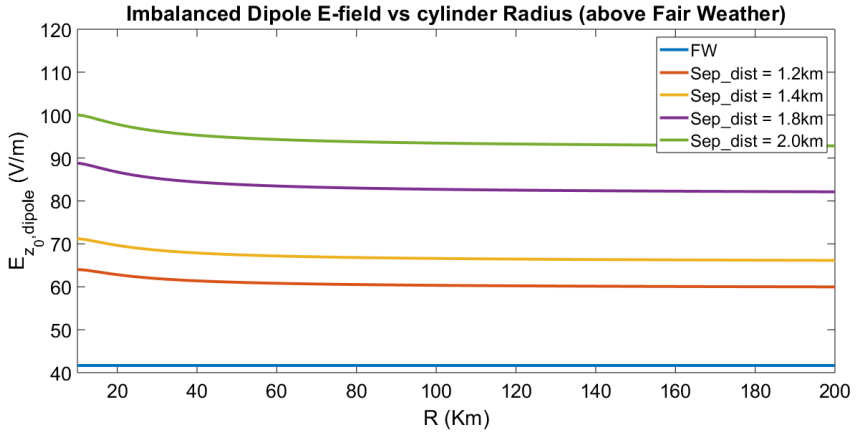

Fig. 12. Vertical electric field strength at ground level for an imbalanced dipole of finite charged cylinders $E_{z_0,dipole}$, within an elevated dust layer as a function of the cylinder radius *R*. The E-field is calculated for separation distances over 1 km between the two charged layers, which results in significant enhancement of the electric field above the fair weather values. The dipole exhibits a charge imbalance of 8%, with the upper negative cylinder having smaller charge density. For these separation distances, the effect to the electric field is significant enough to overcome the calculated fair weather values.

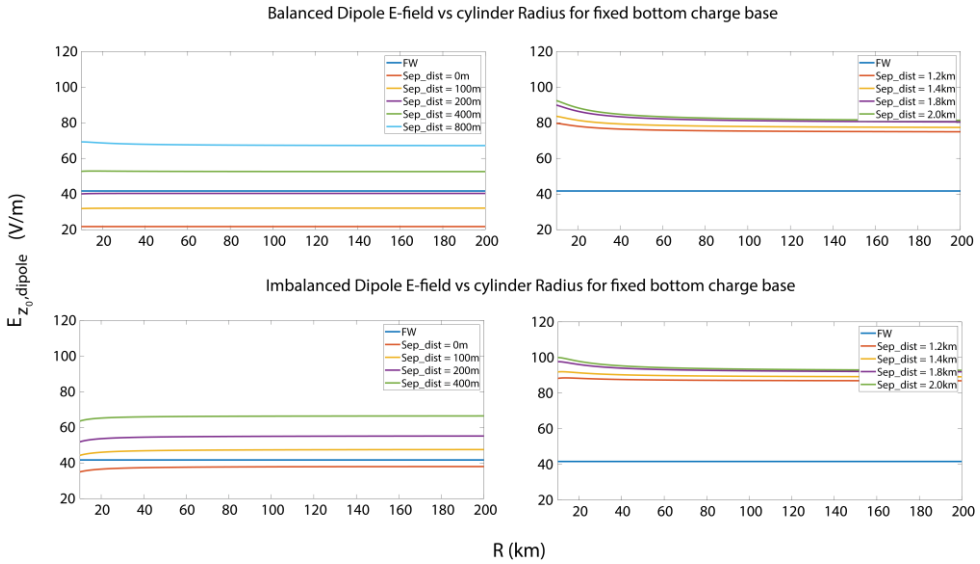

Fig. 10. Dipole electric field strength at ground level $(E_{z_{0,dipole}})$ as a function of the cylinder radius *R*, with the bottom cylinder at 2 km fixed central height within the dust layer. The separation distance between the upper and bottom charged layer increases as the upper cylinder moves towards the top of the dust layer, for both cases of balanced and imbalanced dipoles.

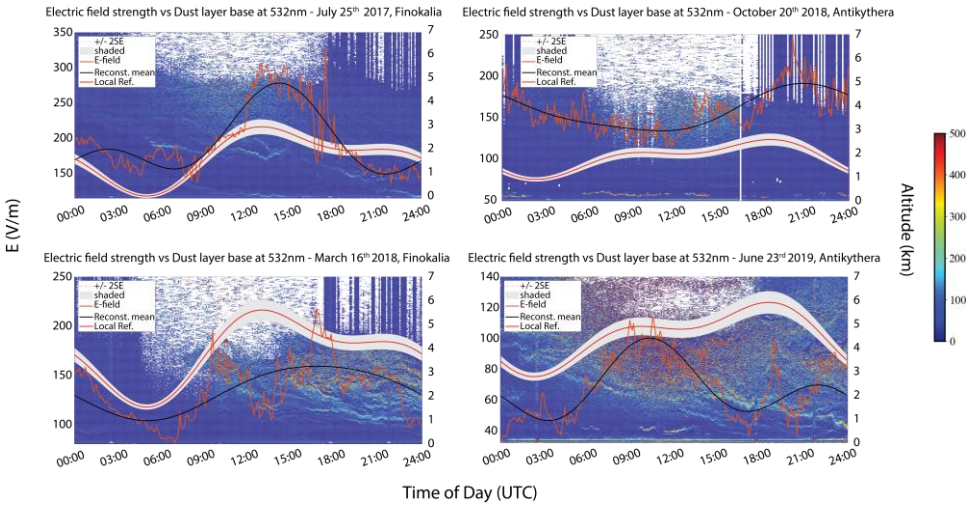

Fig. 11. Timeseries of the vertical electric field strength (orange), the extracted Localized Reference Electric Field (red) and the reconstructed mean field variation (black), plotted with the first derivative of the cross component of the $Polly^{XT}$ attenuated backscatter coefficient at 532 nm against the altitude, for the dust cases of 25/07/2017, 20/10/2018, 16/04/2018 and 23/06/2019. The dust layer bottom base is signified by the positive maximum values of the derivative within the 0 - 500 colorbar range.

Formatted: Superscript

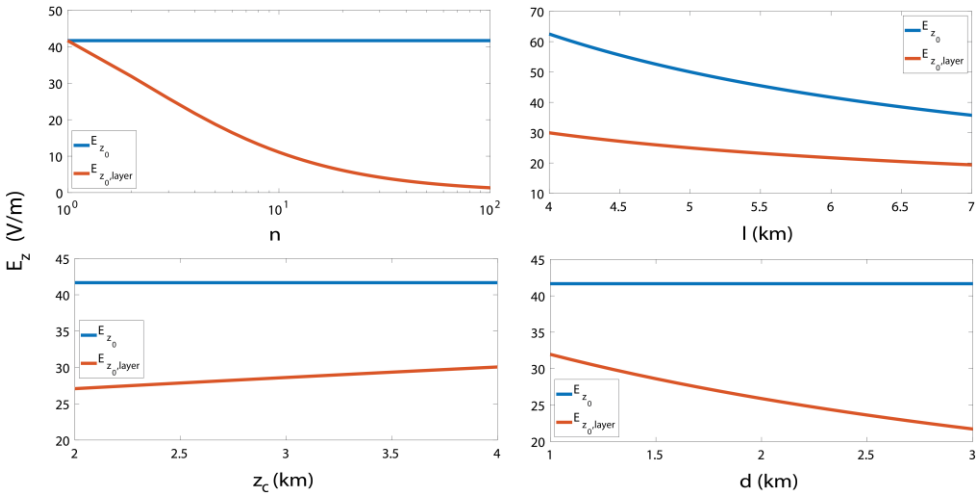

Fig. A1. Dependence of the vertical electric field at ground level, under fair weather (E_{z_0}, blue line) and under the influence of an uncharged dust layer ($E_{z_0,layer}$, red line) on: (a) the reduction factor n, (b) the scaling height l, (c) the central layer height z_c and (d) the dust layer depth d, for $1/\sigma_0 = 3 \cdot 10^{13}\ \Omega\ m$, $V_{ion} = 250$ kV and $H = 70$ km.

~~Fig. 8. Dependence of the vertical electric field, at ground level, under fair weather (E_{z_0}, blue line) and under the influence of an uncharged dust layer ($E_{z_0,layer}$, red line) on: (a) the reduction factor n, (b) the scaling height l, (c) the central layer height z_c and (d) the separation distance d, for $1/\sigma_0 = 3 \cdot 10^{13}\ \Omega\ m$, $V_{ion} = 250$ kV and $H = 70$ km. $E_{z_0,layer}$ strongly depends on the conductivity reduction as depicted in the case (a) curve, where the field reduces with the increasing reduction factor more effectively than with respect to the other three parameters. E_{z_0} depends only on the scaling height as expected.~~

Formatted: Caption, Left, Don't keep with next